







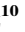







### Special Section:

The Perseverance Rover's  
Exploration of the Western Fan  
Front, Jezero Crater, Mars

## Depositional Facies and Sequence Stratigraphy of Kodiak Butte, Western Delta of Jezero Crater, Mars

G. Caravaca<sup>1</sup> , G. Dromart<sup>2</sup>, N. Mangold<sup>3</sup> , S. Gupta<sup>4</sup>, L. C. Kah<sup>5</sup> , C. Tate<sup>6</sup> ,  
R. M. E. Williams<sup>7</sup> , S. Le Mouélic<sup>3</sup> , O. Gasnault<sup>1</sup> , J. Bell III<sup>8</sup>, O. Beyssac<sup>9</sup> , J. I. Nuñez<sup>10</sup> ,  
N. Randazzo<sup>11</sup>, J. Rice Jr.<sup>8</sup> , L. S. Crumpler<sup>12</sup>, A. Williams<sup>13</sup> , P. Russel<sup>14</sup> , K. M. Stack<sup>15</sup>,  
K. A. Farley<sup>16</sup>, S. Maurice<sup>1</sup> , and R. C. Wiens<sup>17</sup> 

### Key Points:

- New observations on the Kodiak delta remnant were carried out to characterize its detailed facies and stratigraphic architecture
- Three deltaic mouth bars are identified showing 4D succession of depositional settings ranging from deltaic plain to slope to shallow lake
- The first ever sequence stratigraphic framework on Mars shows four cycles of alternating rises and falls of the lake-level within 5–10 m

### Supporting Information:

Supporting Information may be found in the online version of this article.

### Correspondence to:

G. Caravaca,  
[gwenael.caravaca@irap.omp.eu](mailto:gwenael.caravaca@irap.omp.eu)

### Citation:

Caravaca, G., Dromart, G., Mangold, N., Gupta, S., Kah, L. C., Tate, C., et al. (2024). Depositional facies and sequence stratigraphy of Kodiak butte, western delta of Jezero crater, Mars. *Journal of Geophysical Research: Planets*, 129, e2023JE008205. <https://doi.org/10.1029/2023JE008205>

Received 11 NOV 2023

Accepted 19 MAR 2024

### Author Contributions:

**Conceptualization:** G. Caravaca,

G. Dromart, N. Mangold

**Data curation:** C. Tate, S. Le Mouélic,

O. Gasnault, J. Bell III, K. M. Stack,

K. A. Farley, S. Maurice, R. C. Wiens

**Formal analysis:** G. Caravaca,

G. Dromart, N. Mangold, S. Gupta,

L. C. Kah, C. Tate, R. M. E. Williams

<sup>1</sup>Institut de Recherche en Astrophysique et Planétologie (IRAP), UMR 5277, Université Paul Sabatier Toulouse III, CNRS, CNES, Toulouse, France, <sup>2</sup>Laboratoire de Géologie de Lyon-Terre Planètes Environnement, UMR 5276, Lyon, France, <sup>3</sup>Laboratoire de Planétologie et Géosciences, UMR 6112, CNRS, Nantes Université, Université d'Angers, Le Mans Université, Nantes, France, <sup>4</sup>Department of Earth Sciences and Engineering, Imperial College London, London, UK, <sup>5</sup>University of Tennessee, Knoxville, TN, USA, <sup>6</sup>Department of Astronomy and Planetary Science, Cornell University, Ithaca, NY, USA, <sup>7</sup>Planetary Science Institute, Tucson, AZ, USA, <sup>8</sup>School of Earth and Space Exploration, Arizona State University, Tempe, AZ, USA, <sup>9</sup>Institut de Minéralogie, de Physique des Matériaux et de Cosmochimie, UMR 7590, CNRS, Sorbonne Université, Museum National d'Histoires Naturelles, Paris, France, <sup>10</sup>Applied Physics Laboratory, Johns Hopkins University, Laurel, MD, USA, <sup>11</sup>University of Alberta, Edmonton, AB, Canada, <sup>12</sup>New Mexico Museum of Natural History and Science, Albuquerque, NM, USA, <sup>13</sup>Department of Geological Sciences, University of Florida, Gainesville, FL, USA, <sup>14</sup>Department of Earth, Planetary & Space Sciences, University of California Los Angeles, Los Angeles, CA, USA, <sup>15</sup>Jet Propulsion Laboratory, California Institute of Technology, Pasadena, CA, USA, <sup>16</sup>Division of Geological and Planetary Sciences, California Institute of Technology, Pasadena, CA, USA, <sup>17</sup>Earth, Atmospheric, and Planetary Sciences, Purdue University, West Lafayette, IN, USA

**Abstract** High-resolution 2D and 3D data remotely acquired by SuperCam's Remote Micro-Imager and Mastcam-Z aboard the *Perseverance* rover enabled us to characterize the stratigraphic architecture and sedimentary record of the Kodiak butte, an isolated remnant of the western delta fan of Jezero crater. Using these data, we build up on previous interpretations of the butte interpreted as a prograding Gilbert-type deltaic series. We characterize three individual stratigraphic Units 0 to 2 on the eastern and northern faces of the butte. Each Unit displays the same vertical succession of prodeltaic/lacustrine bottomsets, delta slope toesets and foresets, and fluvially influenced topsets of a deltaic plain with a braided river pattern, shown by 11 individual sedimentary facies. We infer that these individual Units record the formation of three distinct deltaic mouth bars successively across time and space. For the first time on another planet than Earth, we are able to construct a precise sequence stratigraphic framework to highlight lake-level fluctuations at the time the Kodiak butte was emplaced, during the latest stages of deltaic activity. We identify four hydrogeological cycles indicated by alternating rises and falls of the lake-level on the order of 5–10 m. These were most probably linked to climatic events and variations controlling lake water inputs in probable relation to an astronomical control.

**Plain Language Summary** Kodiak butte is an isolated remnant of the main western sedimentary fan of Jezero crater. It displays the characteristic structures of a Gilbert-type delta, a structure that shows deposition of fluvial material into a standing body of water, here interpreted to be a lake within Jezero crater. 11 individual sedimentary facies (textures, grain-sizes, and structures) of the rocks exposed at Kodiak suggest that the depositional environments ranged from the fluvial plain to a steep subaqueous slope and into the bottom of the shallow Jezero lake. Our observations further show that Kodiak butte is organized into three distinct stratigraphic Units (0–2), each displaying the same vertical succession of bottomsets, toesets, foresets and topsets. This architecture is interpreted as reflecting three distinct deltaic packages, formed consecutively and not at the same time. Using these facies and stratigraphic architecture data, we are able for the first time on another planet than Earth, to precisely construct a sequence stratigraphic framework for the formation of Kodiak. This framework illustrates with unprecedented precision successive episodes of rises and falls of the paleo-lake-level (in the order of 5–10 m) involved in the construction and evolution of the western Jezero delta.

© 2024. The Authors.

This is an open access article under the terms of the [Creative Commons Attribution License](https://creativecommons.org/licenses/by/4.0/), which permits use, distribution and reproduction in any medium, provided the original work is properly cited.

**Funding acquisition:** O. Gasnault, K. M. Stack, K. A. Farley, S. Maurice, R. C. Wiens  
**Investigation:** G. Caravaca, G. Dromart, N. Mangold, S. Gupta, L. C. Kah, C. Tate, R. M. E. Williams, O. Gasnault, J. Bell III, O. Beyssac, J. I. Nuñez, N. Randazzo, J. Rice Jr., L. S. Crumpler, A. Williams, P. Russel, K. M. Stack  
**Methodology:** G. Caravaca, G. Dromart, N. Mangold, C. Tate, S. Le Mouélic  
**Project administration:** A. Williams, P. Russel, K. M. Stack, K. A. Farley, S. Maurice, R. C. Wiens  
**Resources:** O. Gasnault, J. Bell III, K. M. Stack, K. A. Farley, S. Maurice, R. C. Wiens  
**Software:** C. Tate, S. Le Mouélic, O. Gasnault  
**Supervision:** O. Gasnault, S. Maurice, R. C. Wiens  
**Validation:** G. Caravaca, G. Dromart, N. Mangold, S. Gupta, L. C. Kah, C. Tate, R. M. E. Williams, N. Randazzo, J. Rice Jr., L. S. Crumpler  
**Visualization:** G. Caravaca, C. Tate, S. Le Mouélic, O. Gasnault, J. Bell III, J. I. Nuñez  
**Writing – original draft:** G. Caravaca, G. Dromart, N. Mangold, S. Le Mouélic  
**Writing – review & editing:** G. Caravaca, G. Dromart, N. Mangold, S. Gupta, L. C. Kah, S. Le Mouélic, O. Gasnault, O. Beyssac, J. I. Nuñez, N. Randazzo, S. Maurice, R. C. Wiens

## 1. Introduction

While Mars is presently cold and arid, several decades of observation have now revealed that water ran freely at its surface during the Noachian and Hesperian epochs (>3.5 Ga), a time when Mars certainly held a warmer and wetter global climate (e.g., Arvidson & Catalano, 2018; Carter et al., 2013; Ehlmann et al., 2011; Grotzinger et al., 2015; Kargel, 2004; Malin & Edgett, 2000; Poulet et al., 2005; Rapin et al., 2021). We still do not know exactly how warm the conditions were nor for how long they prevailed. These conditions nonetheless left tell-tale signatures of former aqueous activity: paleovalleys or inverted channels networks (e.g., Burr et al., 2010; Carr, 2012; Hynek et al., 2010), ancient lake beds in craters and chasmata (e.g., Dromart et al., 2007; Edgett & Sarkar, 2021; Grotzinger et al., 2015; Wilson et al., 2010) and many of fan-shaped deposits (Adler et al., 2019; De Toffoli et al., 2021; Di Achille & Hynek, 2010; Morgan et al., 2022; Wilson et al., 2021; Zhang et al., 2023) that have been interpreted as being potential deltas. The term “delta” has been defined on Earth (Nemec, 1990b) as a “deposit built by a terrestrial feeder system, typically alluvial, into or against a body of standing water, either a lake or a sea.” On Mars, such deposits have been observed and identified from orbit in a variety of locations, including Eberswalde crater (Mangold et al., 2012), Gale crater (Palucis et al., 2016), Terby crater (Ansan et al., 2011), and in Jezero crater. In the latter, the geomorphic expression of two sedimentary fans has been documented from orbit along the northern and western margins of the crater (Figure 1a; e.g., Fassett & Head, 2005; Ehlmann et al., 2008; Goudge et al., 2015, 2017, 2018; Schon et al., 2012). Herein, we refer to the term “fan”, which is more generic than “delta” and can include subaerial as well as subaqueous deposition.

Jezero crater is a medium-sized (~45 km in diameter, Figure 1a) impact crater thought to have formed ca  $3.6 \pm 0.1$ –0.3 Ga ago (Mangold et al., 2020 and references therein). It is located at 18°24'N and 77°41'E along the western margin of the Isidis Planitia depression and east of the Nilli Fossae fractured region. The crater rim shows three conspicuous breaches linked to a regionally well-developed fluvial valley network (Figure 1a). The eastern breach (known as Pliva outlet, Fassett & Head, 2005; Figure 1a) is identified as an overflow valley, while the two other breaches (on the northern and western sides of the rim) are interpreted to be inlet valleys associated with kilometer-sized, fan-shaped layered deposits at their mouth (e.g., Goudge et al., 2015, 2017, 2018; Salese et al., 2020). Notably, inferred delta (i.e., sedimentary fan) deposits within Jezero crater bear orbital detection of spectral signatures indicative of the presence of hydrated and/or alteration minerals (e.g., phyllosilicate and carbonate minerals, Goudge et al., 2015; Horgan et al., 2020). The western fan is the largest and best preserved of the two; it sits at the mouth of the largest and deepest breach in the crater rim and is connected to Neretva Vallis (Figure 1), which is inferred to be the source of most of the detrital material in the fan (e.g., Salese et al., 2020). What remains of the fan today covers an area of about 35 km<sup>2</sup>, and displays a variety of morphologies at its surface, including channel belt structures, suggesting a polyphase depositional history (e.g., Kronyak et al., 2023; Stack et al., 2020). By landing in Jezero crater in February 2021 the *Perseverance* rover (and companion *In-genuity* helicopter), the Mars 2020 mission (Farley et al., 2020) was offered an unprecedented opportunity to obtain ground-based data relating to the vertical and horizontal successions of the orbitally defined western fan.

During the first part of its ~22 km traverse (as of October 2023) from the Octavia E. Butler landing site (Figure 1b), the rover gathered numerous remote observations toward the fan front and its surroundings to characterize its sedimentary architecture. Among the observed regions was a rise informally named “Kodiak butte.” Kodiak butte is an isolated flat-topped hill situated about 1 km SSE of the edge of the erosional front of the western fan (Figure 1). It is the largest among several layered topographic features that occur on the Jezero crater floor (e.g., Dragonera, Cabrera, Figure 1b), measuring ~240 m from north to south and ~180 m from west to east. The maximum height of the butte is ~75 m above the local crater floor level (Figure 1d), with the top elevation nearly identical to that of the main fan front (Figures 1c and 1d). The similar elevation and erosional expression observed on both the butte and the main fan (e.g., Gupta et al., 2022; Mangold et al., 2021; Mangold et al., 2024) suggests Kodiak as an erosional remnant that has been isolated from the main fan (cf. Stack et al., 2020).

Mangold et al. (2021) were the first to use *Perseverance*'s ground-based images of the fan front to characterize the sedimentary architecture and morphology visible at the outcrop-scale. Long-distance imaging of the Kodiak butte using SuperCam's Remote-Micro Imager (RMI) allowed them to describe a conspicuous succession of bot-tomsets, foresets, and topsets morphologies at Kodiak. These data confirmed that the western fan in Jezero crater contained deltaic deposits (more specifically associated with Gilbert-type deltas), at least during the timeframe within which the deposition of the Kodiak butte occurred. These deposits have been interpreted by Mangold et al. (2021) to be emplaced within a shallow (~20 m-deep at maximum) lake inside a closed basin system.

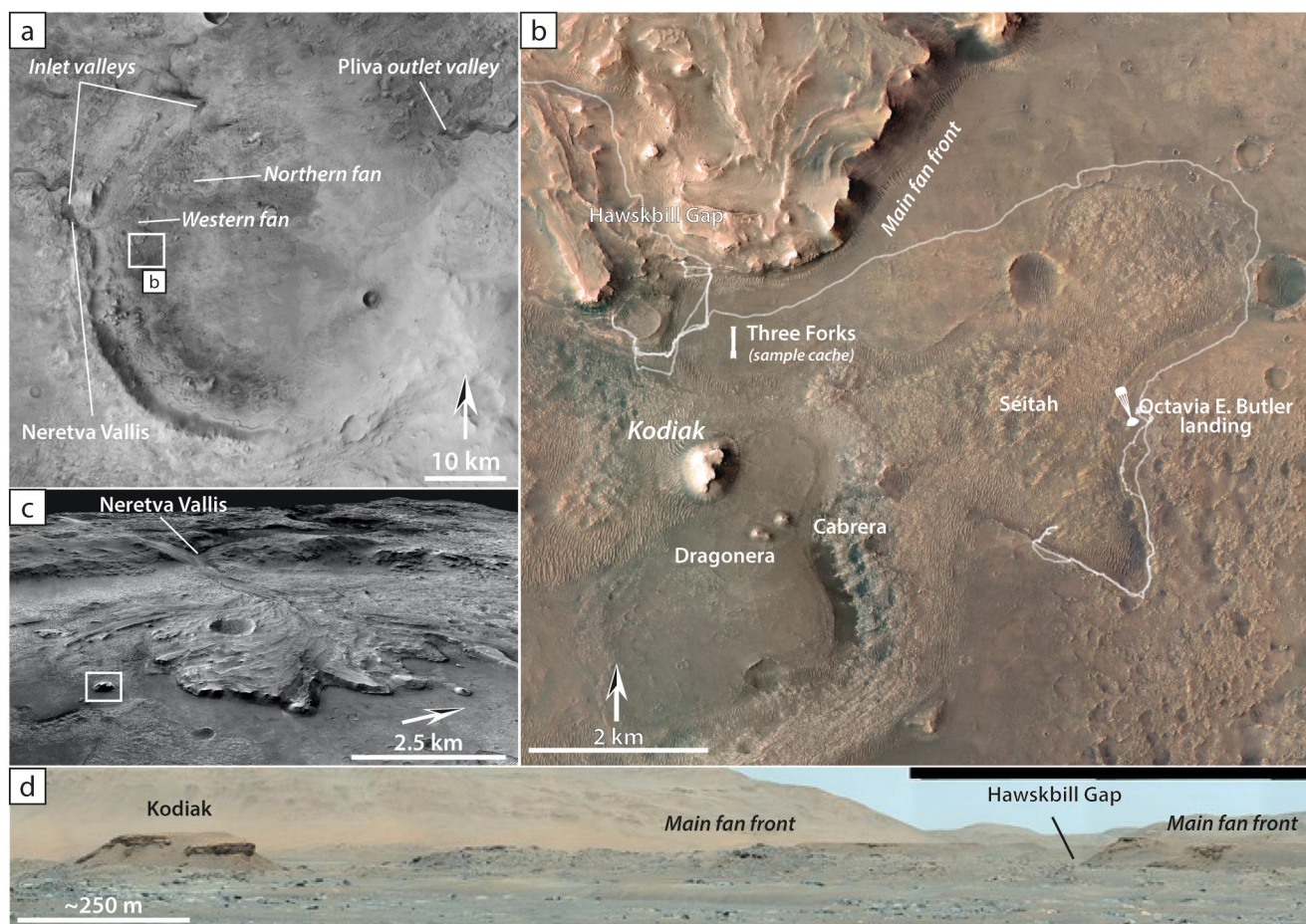


**Figure 1.** (a) General view of Jezero crater along with major geomorphic features of the crater (CTX basemap). The white box corresponds to the study area explored by the Mars 2020 rover *Perseverance* in Jezero crater and is detailed in (b) with main landmarks and the rover's traverse (white line) from the landing site on the crater floor and up the western delta (as of July 2023, color HiRISE basemap). (c) 3D “bird's eye” view of the western delta of Jezero crater at the mouth of Neretva Vallis. White box highlights the Kodiak remnant butte ~1 km south of the current main delta front. (d) General view of the flat-topped Kodiak butte from a distance, with the main fan front in the background (sequence zcam08103).

In this work, we used high-resolution images acquired by the SuperCam's RMI and Mastcam-Z instruments to produce 3D outcrop models and further characterize the details of the exposed sedimentary series of Kodiak butte. These new data acquired along the rover's traverse both east and north of Kodiak complement those previously used in Mangold et al. (2021) and gathered from a unique point of view to the east and around the landing site. Building on previous work from Mangold et al. (2021), we explore observations of the Gilbert-delta geometries and sedimentary facies to identify three distinct episodes of deposition at Kodiak and to decipher the depositional settings that prevailed at the time of Kodiak butte formation. We also propose—for the first time on another planet than Earth—a detailed sequence stratigraphic framework that permits recognition of hydrogeologic cycles associated with variation of the paleo-lake-level in Jezero crater.

## 2. Materials and Methods

The data used to study Kodiak butte were collected remotely by *Perseverance* during the first ~600 Sols of rover activity at times when Kodiak butte was visible to the rover's cameras. These acquisitions provided excellent coverage of the exposed strata at Kodiak butte from many different points of view (see traverse map in Figure 1b). The closest approach to Kodiak butte was ~650 m from the butte; a closer approach was limited by both the restricted trafficability of the nearby terrain, and mission priorities to ascend the fan front.



## 2.1. Instruments and Products

The *Perseverance* rover is equipped with multiple high-resolution color imagers. The Mastcam-Z instrument consists of a pair of two zoomable cameras with filter wheels for multispectral imaging. The cameras can acquire images up to  $1,648 \times 1,214$  pixels with a variable focal length ranging from 26 to 110 mm, allowing for a variety of fields of view from  $25.6^\circ \times 19.2^\circ$  (26 mm) to  $6.2^\circ \times 4.6^\circ$  (110 mm; Bell et al., 2021). The two cameras have a stereo baseline of 24.4 cm, allowing stereo pairs to be acquired when operating at the same focal length to produce 3D models of the observed outcrops and features (Bell et al., 2021; Paar et al., 2023; Tate et al., 2024). The Remote Micro-Imager (RMI) is a subsystem of the SuperCam multi-technique instrument designed to provide high-resolution ( $2,048 \times 2,048$  pixels) context images of the targets investigated by the SuperCam instrument (Gasnault et al., 2021; Maurice et al., 2021; Wiens et al., 2020). When pointed toward long-distance targets ( $>15$  m), SuperCam's RMI is used as a 563 mm focal Schmidt-Cassegrain telescope, allowing images capable of recording cm-scale features at a distance of a few kilometers (Maurice et al., 2021), making it the most powerful imaging device onboard the rover for detailed remote outcrop characterization.

In this study, we use various image products (e.g., individual frames and mosaics) to assess outcrops at Kodiak butte and its immediate surrounding, as well as the local to regional context of Kodiak and its relation to the main fan front (Mastcam-Z). These images enable us to characterize the exposed rocks, outcrop conditions, structures, and textures (Mastcam-Z 110 and RMI), and provide the basic data that permits us to compute 3D Digital Outcrop Models (DOM) of the Kodiak butte (cf. 2.2).

## 2.2. Digital Outcrop Modeling

Image products from the different instruments help give various scales and resolutions, and enable the multi-scale characterization of sedimentary and stratigraphic characters at different levels of detail. However, the architecture and stratigraphic succession of the sedimentary bodies are 3D objects whose spatial distribution and orientation could be critical to decipher the exact mechanisms of formation. To that extent, 3D virtual reproductions of the outcrops are useful. While orbital imaging acquired by the Mars Reconnaissance Orbiter probe (HiRISE instrument) allows the reconstruction of Digital Elevation Models (e.g., Figure 1c), the best resolution of the reconstructed relief is  $\sim 1$  m (HiRISE DEM; McEwen et al., 2007), which is commonly insufficient to resolve individual depositional bodies.

We use Structure-from-Motion photogrammetry (Ullman, 1979) to produce Digital Outcrop Models (DOMs) of the Kodiak butte. This technique is particularly well-suited to perform the computation of accurate, photorealistic 3D models of given outcrops. This technique has been widely used in recent years on Earth geological structures (e.g., Tavani et al., 2014; Triantafyllou et al., 2019) as well as in the Planetary Geology community (e.g., Banham et al., 2022; Barnes et al., 2018; Caravaca et al., 2020, 2021, 2022; Le Mouélic et al., 2018, 2020). These models, based on images taken by the *Perseverance* rover, allow us to reconstruct geological features at Kodiak in 3-dimensions, permitting various points of view, which is particularly helpful since all images were taken from typically more than 700 m away from the butte.

In this study, we mainly used two DOMs of the Kodiak butte computed with the Agisoft Metashape software (v.1.8.5, Agisoft LLC, 2023). The first model (visible on the Sketchfab platform at <https://skfb.ly/o89yU>) reproduces the southeastern part of the Kodiak butte (cf. Figures S1a and S1b in Supporting Information S1). This DOM was computed using long-distance RMI images taken from positions  $\sim 800$  m apart to recreate a virtual stereo baseline (cf. Figure S1c in Supporting Information S1), after a method proposed by Caravaca et al. (2021). This model permits close observation of this area of the Kodiak butte, allowing the spatial characterization and measurement of features as small as 3 cm. Another model (visible on the Sketchfab platform at <https://skfb.ly/oCyI8>) reproduces about two-thirds of the perimeter of the butte (cf. Figure S2 in Supporting Information S1; Tate et al., 2023, 2024) and was made using a long stereo baseline technique with regular Mastcam-Z stereo pairs acquired as the rover traversed around the butte (Figure 1b). This model permits spatial characterization and measurement of exposed sedimentary features and structures larger than  $\sim 15$  cm (see Tate et al., 2024). More information about the specific method and details of this reconstruction are given in the companion work by Tate et al. (2024). Additionally, these models were integrated into a Virtual Reality environment (e.g., Caravaca et al., 2020; Le Mouélic et al., 2018, 2020) to allow their visualization and characterization at varying scales, including true scale.

### 2.3. Key Sedimentary and Stratigraphic Characteristics

The determination of the size, shape, and spatial distribution of sedimentary bodies and structures was carried out using 2D Mastcam-Z and RMI images or using 3D DOMs produced with those images. Scaling on the images varies with distance, but usually allows observation of cm- to decimeter-scale details in Mastcam-Z 110 images (Bell et al., 2021), and cm-scale details in RMI images (Gasnault et al., 2021; Maurice et al., 2021) taken from up to ~2 km away from the target. Accurate measurements of size and orientation were performed using oriented and scaled DOMs, with scale adjustments and accuracy checks performed against high-resolution orbital images from HiRISE (cf. Tate et al., 2024 for details).

Grain sizes are classified according to Wentworth (1922) and Lazar et al. (2015), with sand being represented by clasts smaller than 2 mm, pebbles smaller than 64 mm, and cobbles smaller than 256 mm; any larger clasts are classified as boulders. Grain size of conglomeratic materials was then determined by the long axes of randomly picked clasts within these beds (e.g., Longhitano, 2008; Nemec, 1996). Grain-size and other fine-scale structures were characterized using high-resolution RMI images, with resolution and scaling determined by the exact distance from the target. RMI pixels are 10.1  $\mu$ rad in size (Gasnault et al., 2021; Maurice et al., 2021), which gives an approximate resolution of 1 cm/pixel at a distance of 1 km. These data therefore allow us to identify large pebbles at distances <1 km, and estimate smaller material down to coarse sandstone at closer distances. Smaller grain-sizes cannot be ascertained from these observations.

Bed thickness, dip, and orientation were measured either using 3D DOMs or 2D RMI and Mastcam-Z images when 3D coverage was not available. Measurement on the DOMs was preferred as it allowed thicknesses to be measured orthogonally to the bedding plane. Measurements performed on the RMI DOM (southeastern part of Kodiak) are available in Table S1 in Supporting Information S1. Detailed methods of measurement are also presented in the companion work by Tate et al. (2024).

## 3. Stratigraphic Architecture and Sedimentary Facies of the Kodiak Butte

The sedimentary successions at Kodiak are best exposed along near-vertical cliff exposures on the east-facing (Figure 2a) and north/north west-facing (Figures 2b and 2c) sides of the butte. Here, we characterize the stratigraphic architecture and sedimentary facies of the butte, building on initial observations gathered by Mangold et al. (2021) on the east-facing side of Kodiak only. We describe the macro-scale stratigraphic record exposed at Kodiak butte (Section 3.1). Sedimentary elements such as bedding contacts, truncations, and changes in sedimentary transport directions are then used to distinguish three spatially distinct units (Section 3.2). Then, we identify 11 discrete facies as well as their probable associated physical processes based on apparent grain-size, texture, and sedimentary structures (Section 3.3).

### 3.1. Description of the Exposed Stratigraphic Successions at Kodiak

On the east face of Kodiak, we observe two outcrop sections, similar in both extent and general appearance, separated by scree and regolith (Figure 2a). These two outcrops were first described by Mangold et al. (2021), but new images taken from closer distances to the outcrop enable us to refine previous observations.

The southernmost outcrop (left in Figure 2a) extends laterally over 80 m, and vertically over 20 m. In this part of the butte, we observe (along the trace of log section #1; Figure 2a) a succession comprising ~10 m of low-dipping (~5°) planar beds, passing upwards into ~6 m of steeply (up to ~35°) inclined bedded strata, unconformably overlain by ~10 m of low-dipping (~5°) planar beds. The latter are, in turn, unconformably overlain by a >2 m thick chaotic body of clast-supported and boulder-bearing material incised into the underlying beds. Note that the steeply inclined strata show an asymptotic shape in their lower part, with a conspicuous decrease in their dip angle toward the lower part, as they become laterally nearly indistinguishable from the underlying sub-horizontal beds (white arrow in Figure 2a). All strata dip toward the S/SE.

The northernmost outcrop within the east-facing cliff (right, in Figure 2a) extends laterally over 70 m, and vertically over 25 m, although only about a little more than 15 m are readily observable through scree, loose blocks, and regolith. In this region, we observe (along the trace of log section #2; Figure 2a) a succession of ~10 m of sub-horizontal to low-dipping (~2–5°) planar beds, passing into ~10 m of steeply (up to 30°) inclined bedded strata, unconformably overlain by >2 m of low-dipping (~5°) planar beds, some of which laterally evolve into steeply inclined beds toward the south (green arrow in Figure 2a). All strata dip toward the S/SW.

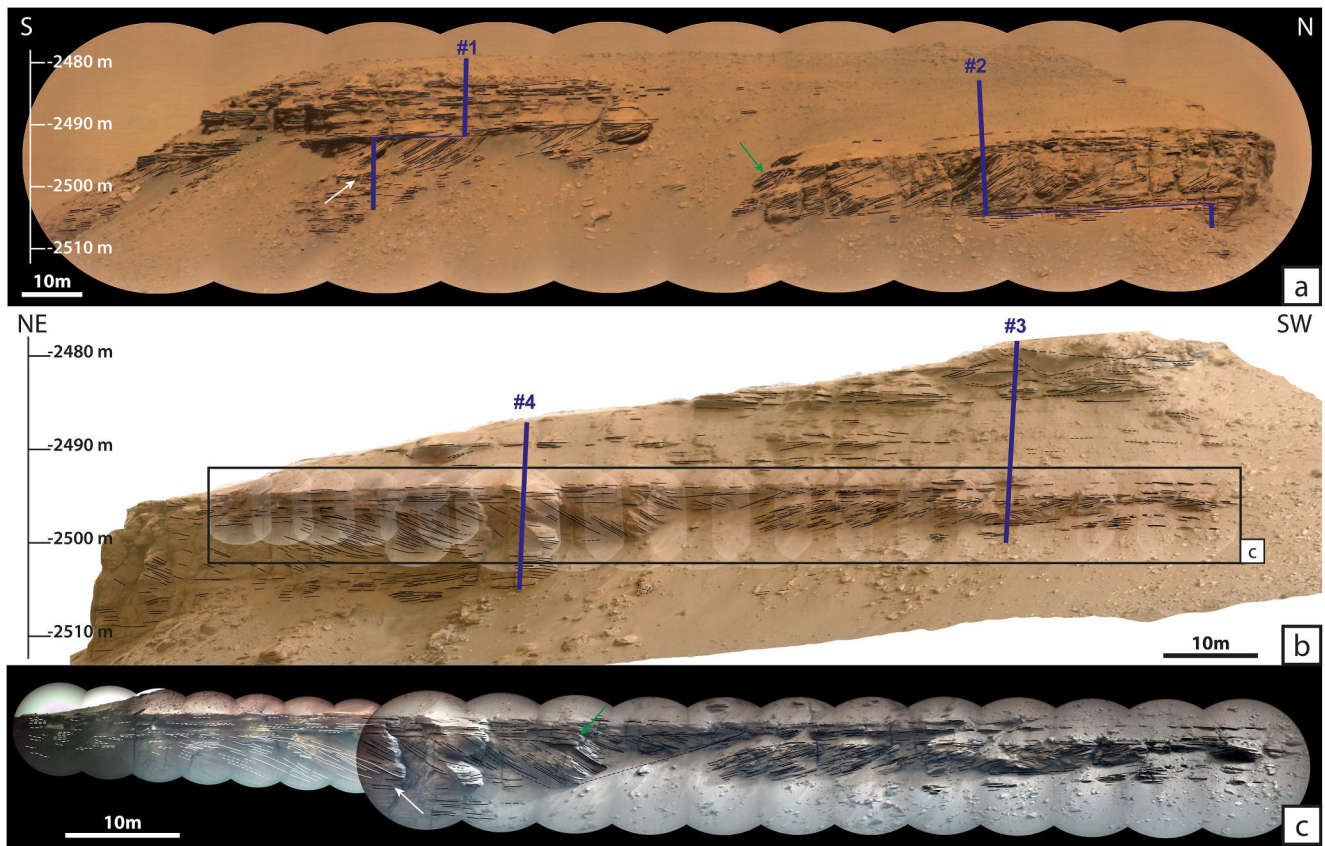


**Figure 2.** (a) General view of the east-facing cliff of Kodiak, with highlights on the main observable geomorphic features in black and position of the log sections #1 and 2 in blue (sequence scam01063). (b) General view of the north/north west-facing cliffs of Kodiak, with position of the log sections #3 and 4 in blue (DOM capture). (c) Detailed view of the main structured part of the north/north west-facing cliffs of Kodiak, with highlights on the geomorphic features in black and white (sequences scam01418 and scam01580). An unannotated high-resolution version of this figure is available as Figure S2 in Supporting Information S1.

On the north/north west face of Kodiak, we observe a single seemingly continuous outcrop in new images (Figures 2b and 2c). Exposure varies greatly along its over 120 m lateral extension with the poorest exposure on the westernmost part of the outcrop (Figure 2b). The observable outcrop spans up to over 20 m in vertical extension (Figures 2b and 2c). We observe (along the traces of log sections #3 and 4; Figure 2b) a vertical succession of ~5 m of sub-horizontal to low-dipping ( $\sim 2\text{--}5^\circ$ ) planar beds, passing into ~7 m of moderately steep ( $\sim 20^\circ$ ) inclined bedded strata, unconformably overlain by ~15 m of low-dipping ( $\sim 5^\circ$ ) planar beds, most of which are obscured by scree and regolith. This uppermost part is then incised by a >2 m-thick chaotic body of clast-supported and boulder-bearing material, similar to the one observed on the east-facing part of Kodiak.

In this region, inclined strata show a conspicuously lower dip angle up to  $\sim 20^\circ$  (Figure 2c) compared to that of the other side (up to  $\sim 35^\circ$ , Figure 2a). Also, we notice two distinct dip directions, wherein the northernmost part of the exposure shows dips toward the W/SW (Figure 2c), whereas the westernmost part of the outcrop shows inclined strata dipping in the opposite direction toward the E/NE (Figure 2c). Similar to what is observed on the east-facing part of Kodiak, we note that inclined strata show an asymptotic shape in their lower part (white arrow in Figure 2c). Low-dipping planar beds both above and below this interval show dip directions toward the W/SW (Figures 2b and 2c). Also, we note that some of the low-dipping planar beds above the observed truncation with the inclined strata laterally evolve into inclined strata at places (green arrow in Figure 2c).

### 3.2. Identification of Individual Units Within the Kodiak Butte

Successions described above do not appear to belong to a single, butte-wide, and laterally continuous sequence. Data from dip directions and continuous elements such as contacts permit identification of three spatially distinct individual units that comprise the stratigraphic architecture.



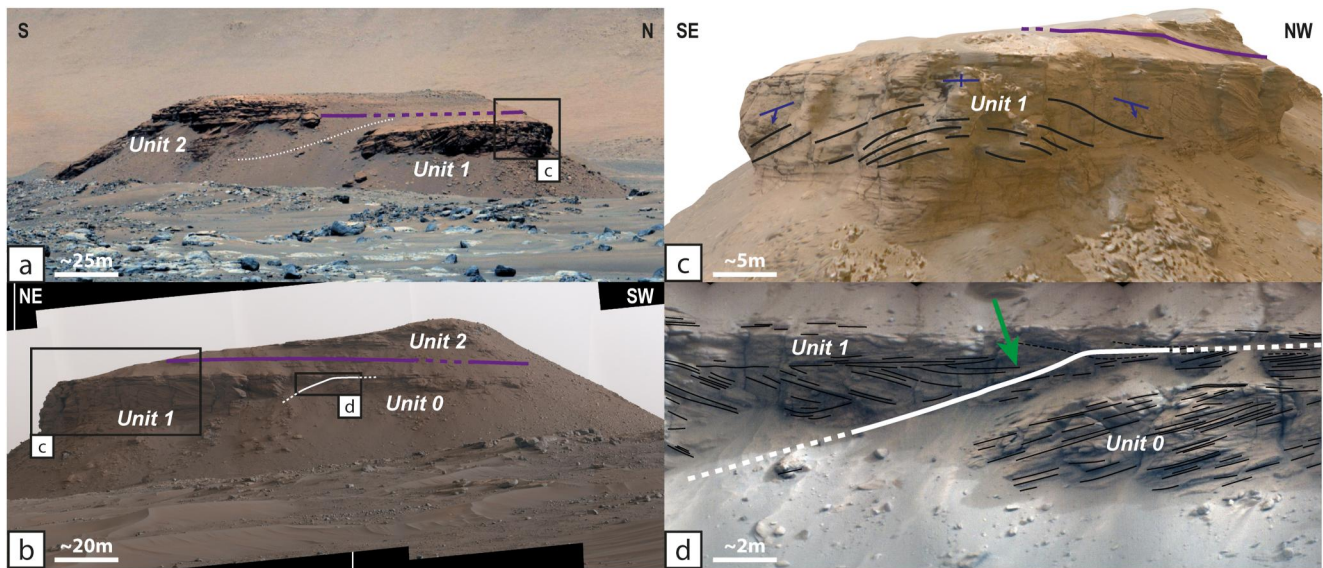


**Figure 3.** Identification of the individual stratigraphic Units 0, 1 and 2. Purple line indicates the location of the marker bed in (a–c) (inferred where dashed). (a) General view of the east-facing part of Kodiak and Units 1 and 2 (sequence zcam08103). (b) General view of the northwest-facing part of Kodiak and units 0, 1, and 2 (sequence zcam08430). (c) Close-up on the northeasternmost corner of Kodiak, as seen using the 3D DOM, exhibiting a conspicuous conical shape architecture, with primary axis oriented toward S/SW. Dip symbols highlight the reversal in dip direction polarity along laterally continuous beds (black lines). (d) Detailed view of the contact between SW-dipping and NE-dipping inclined beds of Units 1 and 0, respectively, on the northern face of Kodiak, with normal, non-erosive onlapping relationship of Unit 1's beds onto Unit 0's. The green arrow points to an example of Unit 1's bed onlapping onto Unit 0's (sequence scam01580).

On the east-facing part of Kodiak, we observe two distinct spatially disconnected outcrops (Figures 2a and 3a). This distinction is conspicuous from both orbit (Figure 1b) and 3D reconstructions (Figure 1c; cf. Figure S2 in Supporting Information S1), which show outcrops do not align on the same vertical (N/S) plane. Additionally, although having a similar thickness, these outcrops do not occur at the same elevation ranges, with the southernmost outcrop observed between  $-2,475$  and  $-2,500$  m, and the northernmost outcrop observed between  $-2,490$  and  $-2,510$  m (Figure 2a). Dip directions of steeply inclined strata also differ, where the southernmost outcrop displays a main dip direction toward S/SE, while the northernmost outcrop shows dips toward S/SW. Finally, we do not observe any correlatable bed(s) between these distinct outcrops. Combined, these arguments strongly support the definition of two distinct—though geologically similar—units from these two outcrops, hereafter referred to as Unit 1 (lower) and Unit 2 (higher) in the stratigraphic succession (Figure 3).

Additionally, we identified a specific  $<1$  m-thick upper planar bed which we used as a “marker bed” (purple lines in Figures 2 and 3). This bed is observed cropping out from the heavily covered upper part of Kodiak above Unit 1 and combined elevation, 2D, and 3D data (cf. Figure S2 in Supporting Information S1) indicate that this bed may be laterally correlatable with the lowermost upper planar beds from Unit 2. Based on this, we infer that Unit 2 is also present above and covering the top of Unit 1 on the east-facing part of Kodiak.

On the north/northwest-facing part of Kodiak, we can easily recognize Units 1 and 2. 3D investigation of the “marker bed” shows its lateral continuity as a planar, nearly undisrupted bed all around the butte (Figures 3a–3c, see also Figure S2 in Supporting Information S1), and shows the presence of Unit 2 on this side of the butte. This is further supported by the strong morphological and geometric similarities between both sides of Kodiak, where Unit 2 shows a thickness of  $\sim 10$ – $15$  m above the marker bed, and is incised by the boulder-rich deposits at the same elevation ( $\sim 2,480$  m, Figures 2 and 3b).

The main exposure on this north-facing part shows a laterally uninterrupted continuation of bedsets from the northernmost outcrop of the east-facing cliff, now referred to as Unit 1 (Figures 3a–3c). On the east, Unit 1's steeply inclined strata are observed to dip toward S/SW, whereas on the north-facing cliff, these inclined strata dip toward W/SW. This seems at first to be incompatible with a single, laterally continuous unit, and Tate et al. (2023) notably showed that this divergence in dip directions can reach up to  $60^\circ$  over 100 m. However, when observed on the 3D outcrop model (Figure 3c), we can observe that the inclined strata are laterally continuous over a  $\sim 25$  m range centered on the northeasternmost corner of the butte where they display a progressive “reversal” of dip

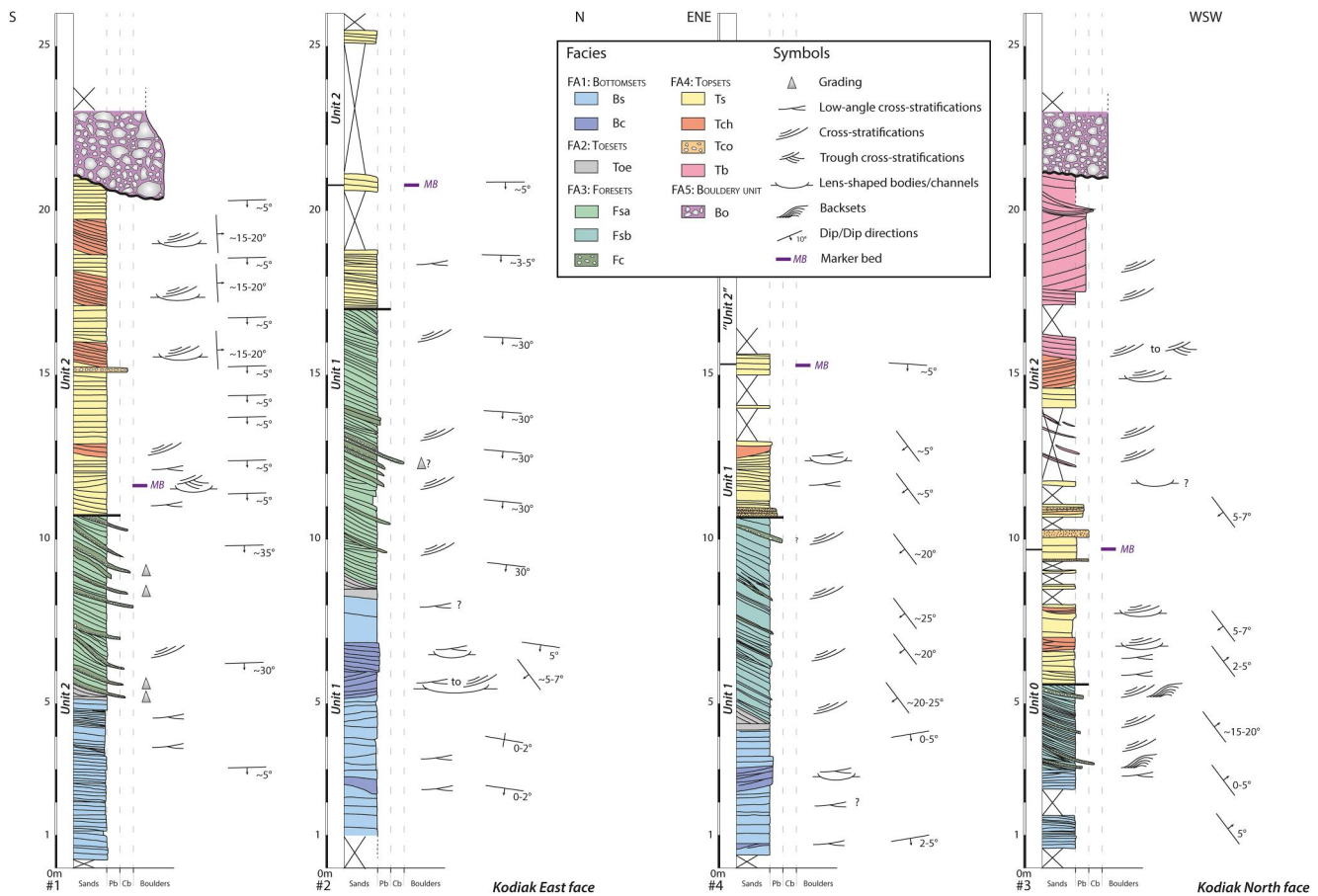


**Figure 4.** Synthetic log sections of the Kodiak butte. Stratigraphic units, facies, main observed sedimentary and geomorphic structures, as well as dip and dip direction are indicated (see also Table 1). FA: Facies associations; Pb.: pebbles; Cb.: cobbles. A high-resolution version of these logs is available as Figure S4 in Supporting Information S1.

polarity (Figure 3c). Unit 1 is therefore recognized on the northern side of Kodiak. Moreover, we characterize a conspicuous conical shape, whose axis (interpreted as the primary transport direction) is oriented toward the south/southwest. This example of bi-directionally dipping, conical-shaped expression of steeply inclined planar beds is not unique to Kodiak, as geometries of the same kind have also been observed on the main fan front by Mangold et al. (2024) at Moro Rock and Whale Mountain outcrops.

Finally, in the westernmost portion of the outcrop, inclined strata show a strikingly different dip direction toward the E/NE while occurring at the same elevation than those from Unit 1 (Figures 2b, 2c, and 3b). Figure 3d shows that these strata seem buried below the W/SW dipping strata of Unit 1. The latter, in turn, are observed to be deposited conformably onlapping (green arrow in Figure 3d). Given the marked difference in dip direction (exact opposite or  $\sim 180^\circ$ ), we can rule out a lateral divergence in dip direction as observed for Unit 1. Therefore, we interpret this westernmost series of E/NE-dipping strata as representative of a distinct unit, hereafter named Unit 0. Similar to Unit 1, Unit 0 is overlain by Unit 2 as recognized by the marker bed (Figure 3b).

### 3.3. Descriptions and Interpretations of Sedimentary Facies Associations

All of the elements developed in Sections 3.1 and 3.2 point toward a general deltaic architecture for the sedimentary successions observed at Kodiak, in agreement with the previous study by Mangold et al. (2021). Taking this into consideration, we distinguish 11 individual facies based on textural parameters (apparent lithology and grain-size) and stratal patterns (bed geometries and structures). They are grouped into 5 facies associations (FA) named using standard deltaic terminology (e.g., Nemec, 1990b). The facies associations are described and interpreted hereafter in ascending stratigraphic order (cf. Figure 4).



### 3.3.1. Bottomset Facies Association (FA1; Bs, Bc)

The Bottomset facies association (FA1, blue-toned colors in Figure 4, Table 1) is present at the base of all sections. The lowermost part of these beds is covered by scree and regolith, so their total thickness cannot be ascertained; however, they comprise at least 8 m of section in Unit 1 (#2 in Figure 4), and more in Unit 2 (Figure 2a). The mean bed thickness within this association is  $\sim 15 \pm 6$  cm (cf. Table S1 in Supporting Information S1). The main facies consists of Bottomset sandstone (Bs, Table 1 and Figures 5a and 5b), which is made of sandstone or finer-grained material organized into planar sub-horizontal low-dipping ( $\sim 5^\circ$ ) beds (blue lines in Figures 5a and 5b). Internally, this facies shows few if any structures. Locally present within Unit 1 (sections #2 and 4, Figure 4) is a coarser-grained variant of this facies, here called Bottomset channels (Bc, Table 1 and Figure 5b). This facies shows estimated grain-size from sand possibly up to pebble conglomerate. It differs from Bs by the exhibition of decimeter-scale 2D cross-stratifications (subdued teal lines in Figure 5b) confined within meter-scale lenticular bedforms with an erosive base contact (dark blue lines in Figure 5b).

Overall, FA1 represents the subaqueous deposition of generally sand-sized sediment within a low-energy setting, potentially resulting from distal waning of gravity-driven currents (e.g., Breda et al., 2009; Nemec, 1990a and references therein). These facies suggest distal turbidity currents near the base of the delta slope within a pro-deltaic lacustrine setting (e.g., Postma, 1986). While Bs represents the potential lowest energy setting of the basal delta slope, Bc marks higher energy deposition. Bottomset channels (Rubi et al., 2018) suggest incision and subsequent infill of channels by intermittent surges of high-density bottom currents, possibly related to episodic floods entering the lake system through the western fan and delta slope.

### 3.3.2. Toeset Facies Association (FA2; Toe)

The Toeset association (FA2, gray in Figure 4, Table 1) is observed in every section except #3, and accounts for less than 1 m in overall thickness (Figure 4). This association comprises only one facies, the Toeset sandstone (Toe; Table 1 and gray lines in Figure 5c), which occurs as thinly bedded, moderately inclined ( $<10^\circ$ ) strata that pinch out laterally. They occur where asymptotic foreset beds become tangential with underlying bottomset beds (transition marked in Figure 5c with color grading from green to gray). Toeset beds locally exhibit some small-scale scours, but no conspicuous unconformity is observed within this FA.

FA2 represents the deposition of sediments at the toe of the delta (lowermost part of the delta slope), which results from the distal waning of gravity-driven avalanches on the slope of the prograding delta (e.g., Longhitano, 2008; Nemec, 1990a). It marks the transition from the deltaic edifice build-up itself into the background lacustrine deposition, potentially evolving into bottomset beds if not buried by progradation of additional toeset beds (Gobo et al., 2014).

### 3.3.3. Foreset Facies Association (FA3; Fsa, Fsb, Fc)

The Foreset association (FA3, green-toned colors in Figure 4, Table 1) is present in all sections and represents up to  $\sim 8$  m of the overall thickness of the stratigraphic succession (#2 in Figure 4). The mean bed thickness for this association is  $\sim 17 \pm 4$  cm (cf. Table S1 in Supporting Information S1). The main facies of this association are Foreset sandstones A and B (Fsa and Fsb, Table 1 and Figures 5c–5f). These facies are composed of sand-sized material and occur in all sections as steeply dipping inclined strata with a sigmoidal shape. The lower portion of this sigmoidal bedding is recognized here as FA2 (Figure 5c). The main distinction between Fsa and Fsb lies in the difference in the dip angle. Fsa beds display overall higher dips up to  $\sim 30\text{--}35^\circ$  (Figure 5d), while Fsb shows less steeply dipping strata with angles between  $\sim 15^\circ$  and  $\sim 20^\circ$  (Figures 5e and 5f). Some localized and poorly expressed examples of meter-scale cross-stratification are observed as well as small-scale scour surfaces (purple line in Figure 5e). Scours seem to be filled by strata displaying sub-horizontal to oppositely-dipping lamination compared to the overall Fsa and Fsb dip directions (purple arrow in Figure 5e). These small structures are identified as probable backsets (*sensu* Massari, 1996; Nemec, 1990b, see also Longhitano, 2008) and are, in these sections, preferentially associated with Fsb.

A coarser-grained variant of this facies, is herein named Foreset conglomerate (Fc, Table 1 and Figures 5d and 5e), which ranges in grain size from coarse pebbly sand up to cobble-sized clasts (individual clasts indicated by green arrows in Figures 5s and 5e, with a mean long axis of  $\sim 23 \pm 10$  cm, up to  $\sim 46$  cm, cf. Table S1 in Supporting Information S1). Cobble-sized clasts commonly occur as discrete, matrix-supported clasts within

**Table 1**

*Sedimentary Facies (and Associations, FA) Observed at the Kodiak Butte*

Facies associations		Texture			Stratal pattern		Settings	
		Facies	Grain-size (apparent)	Matrix/clast support	Bed geometries	Structures	Zone	Energy
Deltaic	1. Bottomset	Bs	Bottomset sandstone	Sandstone (or finer-grained material)	Matrix-supported (cemented?)	Planar beds, low-angle dip (~5°)	Low-angle cross-strata	Low-energy flumes, distal turbidity currents at the bottom of/beyond the Gilbert delta.
		Bc	Bottomset channels	Sandstone to pebble conglomerate	Matrix-supported	Inclined decimeter-scale beds within meter-scale lenses	2D cross-stratification	Mid-energy flumes (linked to floods?). High-density currents at the bottom of/beyond the Gilbert delta; channel filling
	2. Toeset	Toe	Toeset sandstone	Sandstone	Matrix-supported	Thinly bedded, tangential ends of sigmoidal foresets (cf. FA3)	Local scours	Delta toe
3. Foreset		Fsa	Foreset sandstone A	Sandstone	Matrix-supported	High-dip (~30–35°) inclined strata; Sigmoidal beds with tangential ends (cf. FA2)	Cross-stratifications, local scours	Delta slope
		Fsb	Foreset sandstone B	Sandstone	Matrix-supported	Medium/high-dip (~15–20°) inclined strata, locally backsets; Sigmoidal beds with tangential ends (cf. FA2)	Local scours	Delta slope
		Fc	Foreset conglomerate	Pebbly sandstone to cobble conglomerate	Matrix to clast-supported	High-dip (~30°) inclined strata; Sigmoidal beds with tangential ends (cf. FA2)	Interbedding with Fsa and Fsb; normal grading upwards, cross-stratifications and scours	Delta slope

Low-energy flumes, distal turbidity currents at the bottom of/beyond the Gilbert delta.

Mid-energy flumes (linked to floods?). High-density currents at the bottom of/beyond the Gilbert delta; channel filling

Delta toe

Delta slope

Delta slope

Delta slope

Episodic surges of higher-energy gravity-induced flows/avalanches (floods?)

**Table 1**  
*Continued*

Table 1 Continued									
Facies associations			Texture		Stratal pattern			Settings	
			Grain-size (apparent)	Matrix/clast support	Bed geometries	Structures	Zone	Likely processes	Energy
FA	4. Topset	Ts Topset sandstone	Sandstone to pebbly sandstone	Matrix-supported	Planar beds, low-angle dip (~5°). Some beds laterally evolve into steeply dipping sigmoid beds (cf. FA3)	Low-angle meter-scale (trough) cross-stratifications	Deltaic plain	By-pass and inter-channel deposition by dumping of sediment on the distal plain	Medium
		Tch Topset channels	Sandstone to pebbly sandstone	Matrix-supported	Inclined decimeter-scale beds (~10–20° dip with varying dip directions) within meter-scale lenticular bedforms	2D cross-stratification, accretionary bars	Deltaic plain	Channels of braided (to meandering?) river onto the distal deltaic/flood plain	Medium high
		Tco Topset conglomerate	Pebble (to cobble) conglomerate	Matrix- to clast-supported	Planar beds, low-angle dip (~5°)	Cross-stratification, scours	Deltaic plain	Episodic flood sheets on the distal plain	Medium high
		Tb Fluvial plain bars	(Pebbly) sandstone to (μ-) conglomerate	Matrix-supported?	Meter-scale amalgamated ripples	Alternating 2D/3D (trough) cross-stratifications, scours and erosive contacts	Flood plain	Entrenched channels of braided rivers onto the proximal/upper fluvial plain	High
Non deltaic	5. Bouldery unit	Bo (Mega-)breccia	Boulder conglomerate (up to meter-scale boulders)	Clast-supported	Chaotic breccia with erosive base	N/A	Flood plain	(Very) high-energy floods	Very high



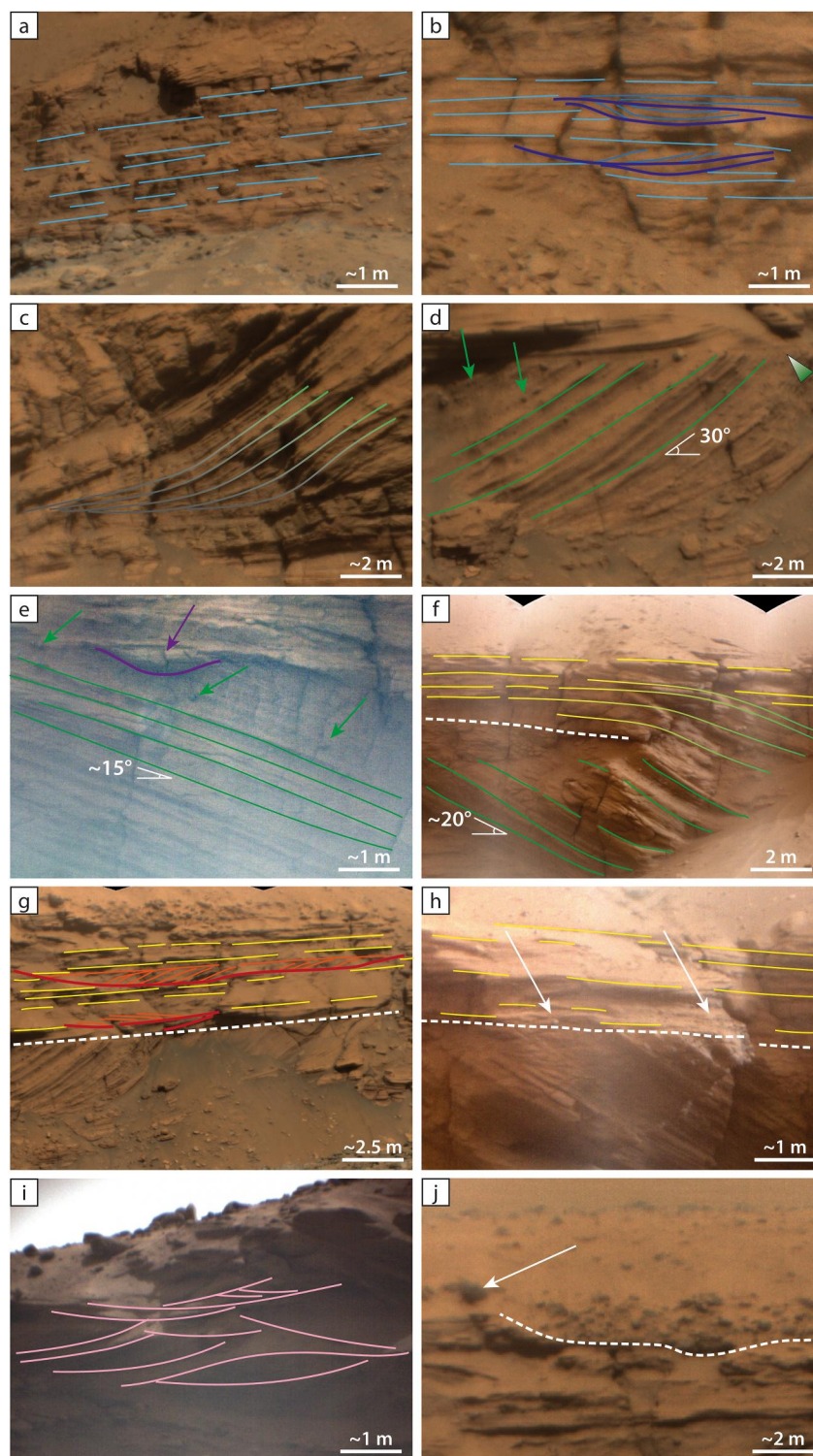


Figure 5.

finer-grained beds (e.g., green arrows in Figure 5e). Fc shows similar bed geometries as Fsa or Fsb, with dip angles to  $\sim 30^\circ$  and an overall sigmoid shape. Fc occurs as individual beds randomly interbedded with strata of Fsa and Fsb. Some individual strata locally show conspicuous normal grading, with cobble to pebble-sized clasts arranged along the bottom contact of the bed, evolving upward into sand-sized material indistinguishable from Fsa and Fsb (green triangle in Figure 5d).

FA3 is interpreted to represent subaqueous, gravity-influenced deposition of non-cohesive grain/debris flows on the slope of the deltaic edifice (Nemec, 1990b and references therein; Postma, 1990). Deposition occurs as sedimentary load on top of the delta becomes gravitationally unstable and avalanches into the lake, and is a primary mechanism of delta progradation (Nemec, 1990b and references therein; Postma, 1990). The presence of individual beds of locally graded, coarser-grained pebble conglomerate interbedded within the sandstone suggests episodic increases in the local energy that could be linked to flood events across the delta (e.g., Bardaji et al., 1990). This hypothesis is also supported by the presence of localized cross-stratification, scour surfaces, and restricted examples of backset beds (e.g., Breda et al., 2009; Postma, 1984). The latter, in particular, are produced by “hydraulic jumps,” a sudden change in flow velocity of the density current responsible for the deposition of the strata (e.g., Longhitano, 2008; Rohais et al., 2008). Another possible explanation for these coarser-grained beds would be their presence as a marker of lags (Dabrio, 1990; Gobo et al., 2015). As short-lived falls in lake-levels would occur, erosion and reworking of higher deltaic layers would lead to reworking of coarser material into the delta slope.

The difference in dip observed between Fsa and Fsb likely reflects the position of the deposits within the 3D deltaic bar. The steeper angles observed (up to  $\sim 35^\circ$ ) are preferentially observed closer to the primary direction of delta progradation, while lower dips indicate a deposition occurring on the lateral banks of a delta bar, off-axis from the primary direction of delta progradation (e.g., Ori & Roveri, 1987; van Yperen et al., 2020; Xu et al., 2023; Zhang et al., 2016). This peculiar 3D architecture is evidenced here at Kodiak within Unit 1 (Figure 3c) as we observe lower dip values associated with the occurrence of Fsb in section #4 compared to Fsa in section #2.

### 3.3.4. Topset Facies Association (FA4; Ts, Tch, Tco, Tb)

The Topset facies association (FA4, yellow to red-toned colors in Figure 4, Table 1) is present in all sections and represents up to  $\sim 15$  m of the overall stratigraphic thickness (#3 in Figure 4). The total thickness varies around Kodiak, and cannot be ascertained as the top of the interval is possibly absent, either removed by incision from FA5 or simple loss to erosion. Also, much of the upper portion of FA4 is covered by scree and regolith, preventing estimation of the total thickness of the interval (e.g., #2 and #4 in Figure 4). The mean bed thickness is  $\sim 19 \pm 5$  cm for planar beds and  $\sim 13.5 \pm 2$  cm for inclined beds (cf. Table S1 in Supporting Information S1).

The main facies of this association is the Topset sandstone (Ts, Table 1 and Figures 5f–5h), that is made of predominantly sand-sized components, although pebbles occur locally. This facies crops out as individual, stacked, planar and sub-horizontal beds (dips  $< 5^\circ$ ), and locally shows some very low-angle, meter-scale cross-stratification. Some beds are observed to laterally evolve into steeply dipping sigmoid beds identified as foresets (FA3, graded yellow to green lines in Figure 5f). However, most of Ts, and more generally most of FA4, show

**Figure 5.** Sedimentary facies observed at the Kodiak butte. (a) Facies Bs, Bottomset sandstone, with low-dipping ( $\sim 5^\circ$ ;  $N = 5$ ) planar sandstone beds (blue lines). (b) Facies Bc, Bottomset channels, exhibiting meter-scale lens-shaped bodies (dark blue lines), with filling of decimeter-scale inclined 2D cross-stratification (subdued teal lines). (c) Facies Toe, Toeset sandstone, with decimeter-scale, asymptotically inclined strata that pinches laterally along a sub-horizontal plane (green to gray lines). (d) Facies Fsa, Foreset sandstone A, with steeply inclined ( $\sim 30^\circ$ , up to  $35^\circ$ ;  $N = 7$ ) asymptotic sandstone beds (green lines). Facies Fc, Foreset conglomerate, characterized by interbedded coarser-grained beds up to cobble conglomerate, as indicated by the large clasts pointed by green arrows. Locally, intrabed normal grading from Fc toward Fsa is observed (green triangle). (e) Facies Fsb, Foreset sandstone B, with less-steeply inclined ( $\sim 15$ – $20^\circ$ ;  $N = 5$ ) asymptotic sandstone beds (green lines). Scour surfaces (purple line) are locally observed and often filled by sub-horizontal and/or opposite-dipping beds interpreted as backsets (purple arrow, *sensu* Massari, 1996; Nemec, 1990b; Longhitano, 2008). Facies Fc is also present interbedded with Fsb (green arrows). (f) Facies Ts, Topset sandstone, with low-dipping ( $\sim 5^\circ$ ;  $N = 15$ ) planar sandstone beds (yellow lines). The base of the Ts interval truncates the top of the underlying Fsa and Fsb strata (white dashed line). Some Ts beds laterally evolve into inclined Fsa or Fsb strata (yellow to green lines). (g) Facies Tch and Topset channels, exhibiting multimeter-scale lenticular bedforms (red lines) with filling of accretionary inclined 2D cross-strata (orange lines). The dashed line represents the truncation of upper foresets (Fsa) by basal topsets (Ts). (h) Facies Tco, Topset conglomerates exhibiting localized decimeter-scale beds of clast-supported pebble to cobble-conglomerate, as evidenced by large-sized clasts pointed by white arrows. (i) Facies Tb, Fluvial plain bars, with meter-scale sandstone to conglomerate beds arranged in amalgamated, alternating 2D/3D megaripples (pink lines). (j) Facies Bo, (Mega-)breccia, as a chaotic, clast-supported, unconformable unit (bottom erosive contact indicated by white dashed line), containing boulders up to  $\sim 1$  m (white arrow). Figure S5 in Supporting Information S1 provides the complete list of original SuperCam's RMI mosaics used for this plate and the location of each excerpt.

a conspicuous erosive truncation between FA3 and FA4 (e.g., dashed line in Figures 5f–5h). This facies also laterally evolves into a facies referred to here as Topset channels (Tch, Table 1 and Figure 5g). Topset channels share most of its characteristics with Ts but crop out as thinner (~13.5 cm vs. 19 cm) inclined beds (orange lines in Figure 5g) that occur within meter-scale, well individualized, locally asymmetrical lenticular bodies with an erosive base and a height no greater than ~80 cm (red lines in Figure 5g). The dip angle of these inclined beds (orange lines in Figure 5g) is generally between ~10° and ~20° and can vary laterally to become near horizontal (lower example in Figure 5g). Dip directions also vary (sometimes strongly) from one individual lenticular body to another.

Locally interbedded within the above facies is a coarser-grained Topset conglomerate facies (Tco, Table 1 and Figure 5h). The Topset conglomerate facies is one of the most poorly expressed facies. It shares most of its characteristics with Ts but is composed of coarser materials that range from pebble- to cobble-sized (white arrows in Figure 5h). Tco does not conspicuously show any grading or imbrication in the available images.

The final facies of FA4 is the Fluvial plain bar facies (Tb, Table 1 and Figure 5i), which is present only in section #3 (Figure 4). This facies is coarse-grained, ranging from (pebbly) sandstone to conglomerate, and appears to be mostly matrix-supported. Tb also differs from Tco in its bed geometries: wherein Tb exhibits well-expressed amalgamated, meter-scale megaripples with alternating 2D and 3D cross-stratification, scours, and erosive contacts that are not apparent in Tco (pink lines in Figure 5i).

Overall, FA4 shows a striking variability in the depositional processes compared to FAs 1 to 3. Increased variability is, notably, associated with a mostly unconformable relationship between FA3 and FA4 (e.g., Mitchum et al., 1977). The topsets are noticeably deposited by different processes linked to subaerial, fluvial-dominated settings in the deltaic plain, as compared to subaqueous, lacustrine-dominated processes of the bottomset, toe-set, and foreset FAs. The lateral evolution of some topset beds into foresets (Figure 5f) confirms a genetic relationship between these FAs.

More specifically, Ts, Tch, and Tco likely represent an ensemble of facies characteristic of a flood plain setting. With poorly expressed structures and sub-horizontal bedding, Ts represents the background deposition in a fluvial (delta) plain setting, dominated by by-pass and dumping of material in inter-channel space (e.g., Allen, 1982; Jones et al., 2022; Miall, 2014). Tch is observed as a filling of lenticular-shaped individual bodies entrenched and carved into the sub-horizontally lying materials characteristic of Ts. This facies also shows the small-scale rather steeply (10–20°) inclined thinner beds within these lenticular bodies that represent lateral accretion of small-scale point bars (e.g., Ghinassi et al., 2016). Finally, Tco represents the highest energy conditions as the coarser-grained facies, but the planar-bedded geometries of its beds indicate an overall non-constrained depositional setting. This facies would therefore represent surges in energy, potentially linked to flood episodes (Allen, 1982; Miall, 2014). Alternatively, variations in supply could also explain the presence of coarser-grained material.

Facies Tb occurs at the highest stratigraphic level at Kodiak. The larger scale (several meters of wavelength) of its 2D and 3D amalgamated cross-stratifications, and the numerous scours and contacts indicate a very high energy setting, possibly the highest of all the previous FAs. This represents a likely “cut and fill” scheme (*sensu* Longhitano, 2008) compatible with a more proximal braided river (delta) plain setting.

### 3.3.5. Bouldery Unit (FA5; Bo)

Facies association FA5 represents the Bouldery unit, and is exclusively observed in the uppermost reaches of Kodiak butte (>–2,480 m in elevation), though not observed in all of the sections (restricted to #1 and #3, Figure 4). The only facies of this FA is the (Mega-)breccia facies (Bo, Table 1 and Figure 5j). It is composed of boulder conglomerate, with clasts showing a mean long-axis measurement of  $\sim 52 \pm 23$  cm, and including boulders up to 104 cm (white arrow in Figure 5j; cf. Table S1 in Supporting Information S1). Bo does not exhibit any conspicuous bed geometry or structure, but rather is represented by a very chaotic and poorly sorted sub-rounded clast content. The base of this breccia interval is systematically observed as unconformable and highly erosive (dashed line in Figure 5j), making meter-scale deep incisions over tens of meters into the underlying FA4 deposits (cf. Figures 2a and 2b).

FA5 represents highly energetic conditions marked by the chaotic deposition of large and poorly sorted boulders. It likely results from powerful but episodic floods. These events likely do not pertain to the deltaic suite, as these



deposits are sporadically observed on top of the butte, and systematically with an unconformable and erosive relationship with the underlying facies (Ts and Tb in sections #1 and #3, respectively, Figure 4).

#### 4. Interpretations of the Deltaic Depositional Environments of Kodiak Butte

The sedimentary succession in Kodiak butte is interpreted to display a wide range of depositional environments, both representing subaqueous (prodelta, delta slope) and subaerial (delta plain) settings. These settings are characteristic of a Gilbert-type delta suite, and their repeated stacking pattern, as observed around Kodiak, argues in favor of a multiphase depositional history. Each Unit represents a single episode of distinct deltaic mouth bar build-up.

##### 4.1. Interpretation of Kodiak Butte as an Isolated Gilbert-Delta Remnant

Conspicuous repetition of a similar sedimentary architecture occurs across the Kodiak butte, displaying a repeated vertical succession of (a) low-dipping planar beds, (b) steeply inclined and sigmoid-shaped strata, and (c) another set of low-dipping planar beds. The latter are mostly observed to rest unconformably onto the underlying sigmoid strata. These successions are similar in size vertically ( $\sim 10$ – $15$  m-thick; Figure 2). In each case, inclined strata have a clear asymptotic shape at the base as well as a sharp, laterally discontinuous truncation between the inclined strata and the overlying planar beds. In Unit 1, such beds are best described as having a conical shape, which is highlighted by the progressive variation in dip and dip-direction between the east- and north/north west faces of the butte (Figures 3a–3c).

Facies show that the deposits observed at Kodiak butte are detrital in origin, and for the most part coarse-grained (ranging from sand- to cobble-sized clasts). Their deposition is inferred to have occurred primarily in subaqueous settings driven by gravity-induced transport (settling, avalanches in FAs 1 to 3) and, for the upper facies in each succession (FA4), in a subaerial fluvial setting.

Overall, the variety of structural and textural elements described here are most consistent with the sedimentary record of a steep-fronted Gilbert delta system (e.g., Breda et al., 2009; Clauzon et al., 2015; Longhitano, 2008; Postma, 1984, 1990; Sztanó et al., 2010). This interpretation is preferred over alternative hypotheses, such as the inclined bedding resulting from subaqueous dunes or lateral accretionary bars in a fluvial setting in the absence of conspicuous scouring surfaces or grading across the interval (cf. Ghinassi et al., 2014, 2016). Moreover, the appreciable size of the foresets ( $\sim 10$  m-thick for  $>70$  m-long) is incompatible with most fluvial settings. For instance, on Earth, comparable sizes are achieved within fluvial systems such as the Mississippi (e.g., Clift et al., 2019), which is unlikely to be achieved within the short distance ( $\sim 7$  km; Figure 1) and relatively small topographic change ( $\sim 300$  m) from the Jezero crater rim to the Kodiak butte. Additionally, flow rates of rivers like the Mississippi are  $> \sim 28,000 \text{ m}^3 \cdot \text{s}^{-1}$  (e.g., Knox, 2013) when maximum estimated rates obtained on the basis of transported boulder size on the main delta front are of  $< \sim 500 \text{ m}^3 \cdot \text{s}^{-1}$  (Mangold et al., 2024).

High-resolution analyses, including our additional observations in the northern part of Kodiak butte, therefore support the previous interpretation by Mangold et al. (2021) regarding the Gilbert-type delta nature of Kodiak butte strata. Finally, the detailed observation of the geometry of beds allows us to clearly diagnose the toeset beds of these stacked deltaic sequences (cf. Figure 5c; Gobo et al., 2014; Longhitano, 2008; Nemec, 1990a), which were previously unrecognized.

##### 4.2. Depositional Model and Paleoenvironments

We propose a new depositional model (Figure 6) accounting for the entire observed succession at Kodiak. It is proposed as a 2D transect along a dip-parallel Gilbert-type delta system, with the classical tripartite succession of bottomset, foreset (and toeset), and topset beds (e.g., Breda et al., 2009; Fayol, 1886; Gilbert, 1885; Gobo et al., 2014; Longhitano, 2008) corresponding to depositional environments ranging from prodelta to delta toe, delta slope and finally delta plain (in ascending stratigraphic order). These environments are associated with FAs defined based on their texture and bed geometries as well as inferred physical processes responsible for the transport and deposition of material.

Within this framework, Bottomset beds of FA1 represent lacustrine settings located in the prodelta part of the Gilbert-delta system (Figure 6). Planar parallel aggrading geometries of these sand-sized (or finer) detrital beds indicate formation in a quiet subaqueous setting beyond the foot of the main deltaic edifice. It represents the

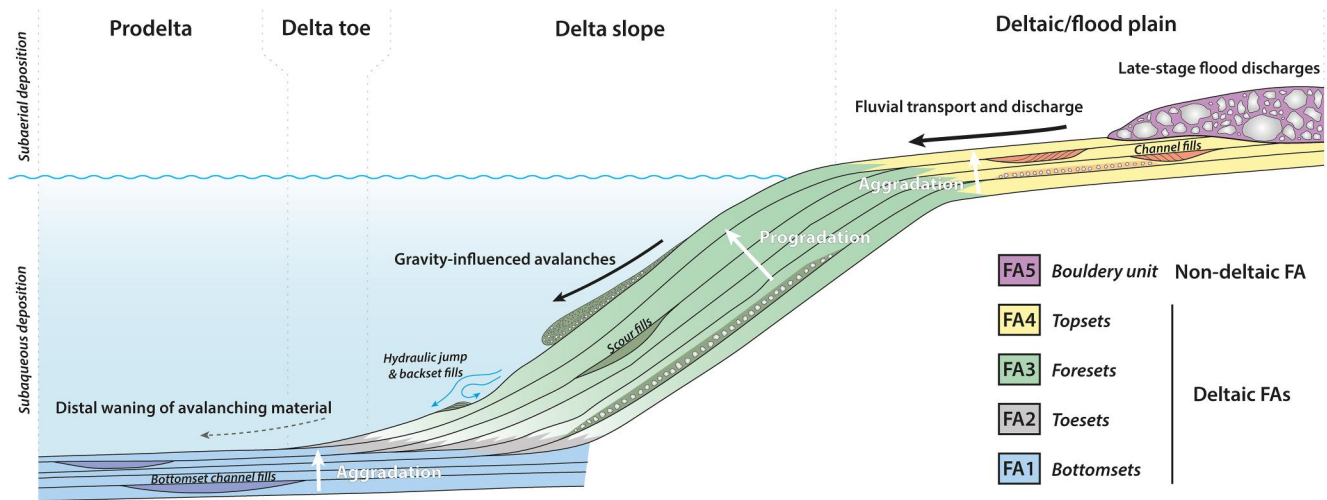


**Figure 6.** 2D schematic representation of the depositional model of Kodiak butte (not to scale). The model shows interpreted paleoenvironmental settings and inferred processes controlling the deposition of the deltaic (FA1 to 4) and non-deltaic (FA5) facies associations observed around the butte.

background lacustrine deposition, most likely related to the deposition of suspended load from the distal waning of density turbidity currents induced by the gravity-driven avalanching sediments on the slope. In places, meter-scale lens-shaped bodies are observed and are interpreted as “bottomsets channels” (e.g., Rubi et al., 2018), a feature related to incision and filling by bedload within low-sinuosity channels (Figure 6). Episodic surges in the energy might be related to flood episodes entering the delta system or local destabilization of the sediment pile in topographically higher portions of the deltaic system.

The delta toe and slope are represented by Toeset (FA2) and Foreset (FA3) facies associations (Figure 6), wherein toeset beds represent the lateral and distal tangential ends of sigmoidal foreset beds. Sedimentary transport and deposition of these beds are associated with density currents (hypo- and hyperpycnal flows), wherein gravitational instability drives avalanches of material onto the slope and down to the delta toe (Figure 6, e.g., Nemec, 1990a; Nemec & Steel, 1984). The recurrence of these deposits reflects their prograding nature. Episodically, density flows or coarse-grained bedload results in scouring the surface of the slope (e.g., Uličný, 2001). Sudden changes in flow velocity or turbulent conditions along the delta slope would also result in the occurrence of hydraulic jumps (e.g., Longhitano, 2008; Rubi et al., 2018), generating scours with concurrent filling of backset strata exhibiting an opposing dip direction compared to the overall foreset strata (Figure 6). The observed size of the Toeset and Foresets packages ranged from approximately 5 to 10 m (Figure 4). This also indicates that their deposition occurred in a shallow lake whose depth would not exceed 10 m at that time.

Topset beds (FA4) mark a striking change in depositional setting to that of the subaerial delta plain (Figure 6). In this setting, fluvial processes dominate to produce a planar-parallel aggrading record characteristic of a braided river plain (e.g., Miall, 2014). This is particularly well evidenced by the recurring presence of meter-scale lens-shaped bodies filled with inclined strata that are interpreted as accretionary bars (e.g., Ghinassi et al., 2014, 2016). These bar deposits illustrate the onset of (possibly meandering) channels that incise the delta plain, no deeper than 1 m at maximum given their observed size. These rivers are considered the main source of the sedimentary material transported onto and then deposited as part of the deltaic system. The nature and energy involved in the fluvial setting vary greatly, with inter-channel sand-sheets representing the quietest fluvial plain setting, and amalgamated 2D and 3D meter-scale megaripples indicating periods of very high river activity.

Finally, the non-deltaic Bouldery unit (FA5) represents deposition that post-dates the deltaic succession of Kodiak butte, observed to take place on top of the deltaic units (Figures 6 and 7). The chaotic, clast-supported material in this FA is similar in character to other boulder conglomerate suites observed on top of the main delta front (Mangold et al., 2021, 2024) and mapped as the “Delta blocky unit” (Stack et al., 2020). FA5 could therefore represent a later stage of fluvial-deltaic deposition (potentially associated with deposits further in the crater but now lost to erosion), or that it is separated by substantial time and is therefore not directly related to the fluvial-deltaic materials seen in Kodiak butte. Mangold et al. (2024) notably argue that the boulders they

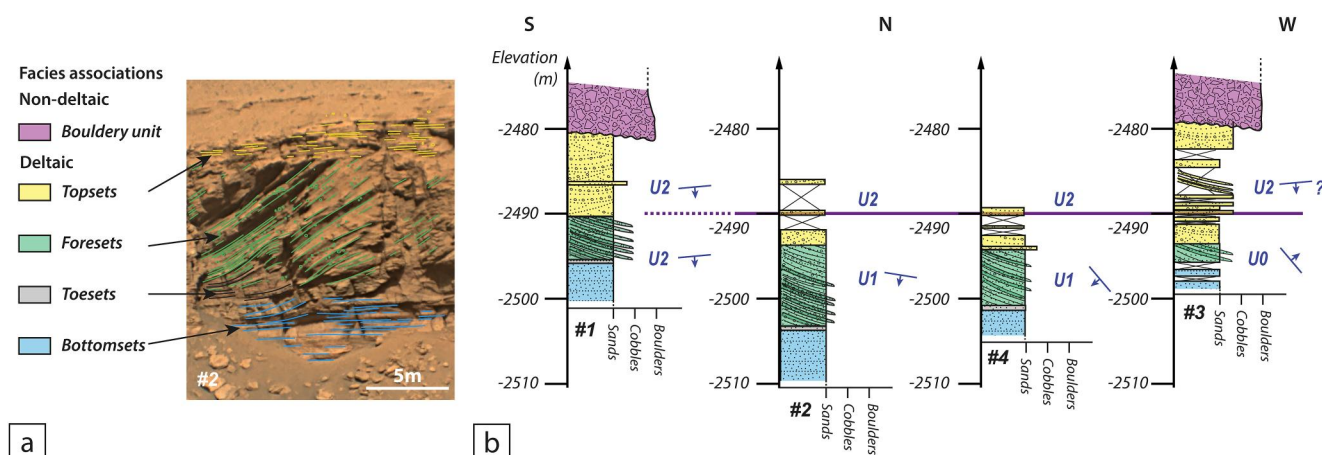


**Figure 7.** (a) Example on the east face of Kodiak of the characteristic vertical stacking pattern of facies associations 1 to 4 interpreted as a deltaic succession (sequence scam02077). (b) Correlation of synthesized log sections of Kodiak indicating the lateral and vertical distribution of the deltaic sequences associated with Units 0 to 2 around Kodiak, and their main transport directions as observed at the outcrop. Purple line denotes lateral correlation between sections tied to the marker bed identified all around the butte.

observe on the main delta front, only a few km away from Kodiak, could be linked to extreme flooding events in the very latest stages of Jezero's fluvial history.

### 4.3. Deltaic Successions of Kodiak

We identify the continuous (either vertically and/or laterally) uninterrupted stacking of FA1 to FA4 (Figure 7a) as an individual deltaic succession (e.g., Breda et al., 2009; Nemec, 1990b; Postma, 1990 and references therein). Each such succession records the progressive local paleoenvironmental change during the progradation of the deltaic system. In that, we can consider that each succession reflects a single episode of deltaic progradation and build-up of a deltaic mouth bar (*sensu* Van Yperen et al., 2020). Coarse-grained Gilbert-delta systems are known on Earth to notably display varying main transport directions across their different mouth bars (e.g., Somoza et al., 1998; Sztanó et al., 2010; Van Yperen et al., 2020). This chaotic pattern mainly results from interactions between local accommodation and variation of the fluvial inputs (e.g., Viparelli et al., 2012). As a consequence, individual mouth bars can be characterized not only by their spatial distribution (location, elevation range) but also by their main sedimentary transport direction, and the stratigraphic relationship to other geomorphic features such as previous mouth bars and/or paleotopography that will control their emplacement (in addition to accommodation which is the space available for the deposition of sedimentary material; e.g., Bardaji et al., 1990; Longhitano, 2008; Somoza et al., 1998). Around Kodiak, we observe that each Unit shows a vertical stacking pattern identifiable with a deltaic succession but also distinct transport directions (Figure 7). This means that, at Kodiak, each single Unit is to be associated with one deltaic succession and henceforth to be considered as the record of a single episode of deltaic build-up (1 Unit = 1 mouth bar). The Kodiak butte itself, recording 3 seemingly amalgamated mouth bars, can be identified as a mouth bar complex (*sensu* Van Yperen et al., 2020).

The identification of the three distinct mouth bars raises the question of their relationship in space and time, including their relative emplacement. Unit 0 (section #3, Figure 7b) occurs at the lowest elevation range (<-2,490 m, Figure 7b), and displays a strikingly different main transport direction toward the ENE compared to other units. We also observe that it is buried under Unit 1 (Figure 3d), and is the least developed (possibly being at times in a more distal position regarding the overall delta system). We thus infer that it was the first emplaced. Unit 1 (sections #2 and 4, Figure 7b) is deposited along a mainly SW-oriented axis, and some of its foresets onlap Unit 0 (Figure 3d), showing a later stage of deposition, even if being observed in a similar elevation range (<-2,490 m, Figure 7b). We also infer that some of Unit 1's topsets could possibly overlap topsets from Unit 0, but the outcropping condition makes this assessment difficult to certify (e.g., Figures 2b and 2c). This indicates that Unit 1 was seemingly the second mouth bar to have been formed at Kodiak. Last, Unit 2 (all sections in Figure 7b, but mainly #1) shows a main direction of transport toward the S/SE and occurs at the highest elevation range (<-2,480 m, Figure 7b). Unit 2 most certainly records the last deltaic stage in the polyphase history of Kodiak formation as it is also the most extensively preserved around the butte. We notably observed its topsets covering



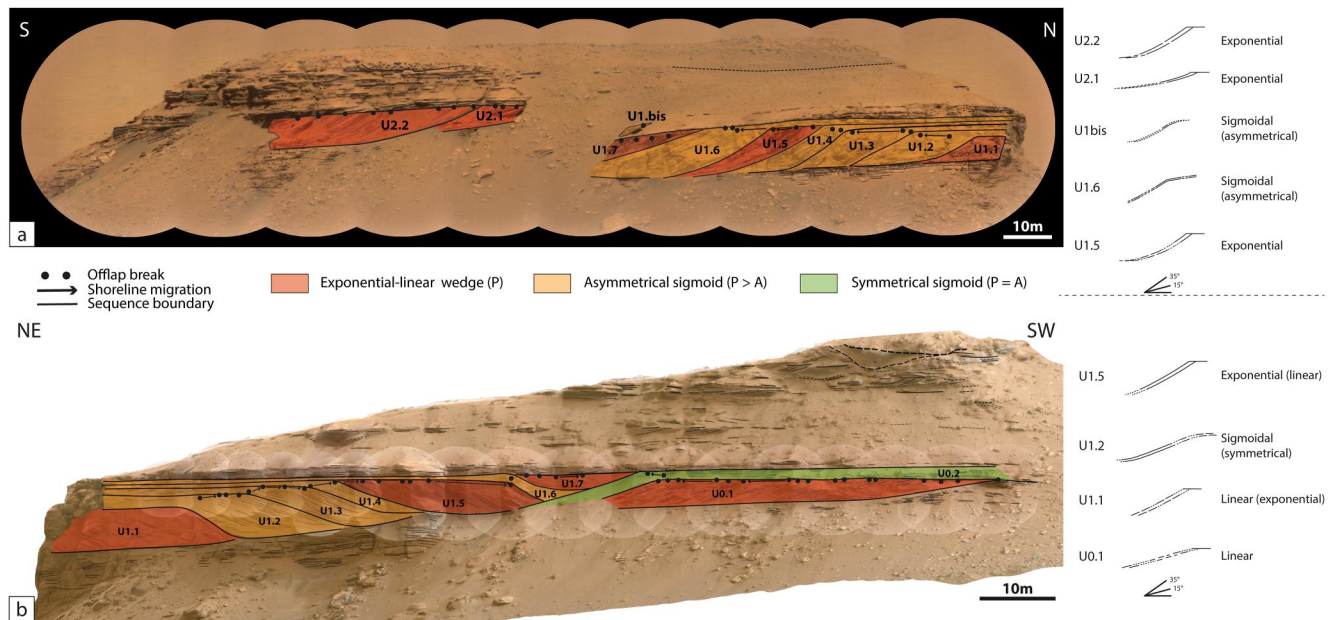


**Figure 8.** Identification of (sub-)unit-scale sequences and their various exponential, linear or sigmoid profiles (right; obtained on the basis of true-scale bed tracing) on east-facing (a) and north-facing (b) faces of Kodiak. Offlap breaks and corresponding inferred shoreline migrations are also represented for each (sub-)unit.

most of the butte's roof, as illustrated by the “marker bed” associated with the topsets of Unit 2 in log section #1 and identified on every other log section (purple line in Figure 7b). We propose that some of Unit 1's topsets, given their dip, could laterally evolve into Unit 2's bottomsets (Figure 2a), indicating a close succession in-between Units 1 and 2.

## 5. Sequence Stratigraphy Framework and Characterization of Variations of the Lake-Level

Accommodation, is usually defined and controlled by two sets of parameters: subsidence and the position of base-level (e.g., Schlager, 1993). On Mars, the crust is anomalously thick and there is no indication of active tectonics at the local scale considered here, making subsidence a negligible factor (Grotzinger et al., 2013). This leaves only fluctuation of base-level (or, in the case of a crater lake, lake-level) as a driver for creation and removal of accommodation. We therefore use the stratigraphic architecture of the deltaic deposits of Kodiak butte to propose a sequence stratigraphic model that describes the 4D evolution of the delta at the time of Kodiak formation. We notably use the foresets/topsets transition as a proxy to map the paleo-base level (e.g., Chavarrías et al., 2018).

### 5.1. Stratal Geometries

In typical Gilbert-type deltas, the geometric transition recorded between foreset and topset beds is referred to as an offlap or slope break. In the case of Jezero crater, where this transition also marks the change from subaqueous (delta) and subaerial (fluvial, delta plain facies), this transition also represents the paleo-shoreline of the deltaic system, which is observed to laterally and vertically migrate through time and space (Figure 8). The spatial movement of these offlap breaks therefore traces the migration of the shoreline and permits reconstruction (via geometries of the foresets) of the paleogeomorphology of the delta front.

Based on true-scale bed tracing on Mastcam-Z and RMI mosaics (Figure 8), we performed a shoreline trajectory analysis. Three types of slope curvature have been recognized for the delta slopes of Units 0 to 2 following the classification proposed by Adams (2001): linear (or planar), exponential (or concave-upward), and sigmoidal (cf. Figure 8). Planar profiles have a straight morphology with a slope angle remaining constant that is assumed to represent the angle of repose. Exponential profiles are composed of straight planar upper foresets (i.e., linear profiles) that flatten out exponentially at the base. The exponential trend is attributed to the exponential decay of transport capacity and competence and is typical of prograding deltas for which the water depth is nearly constant.

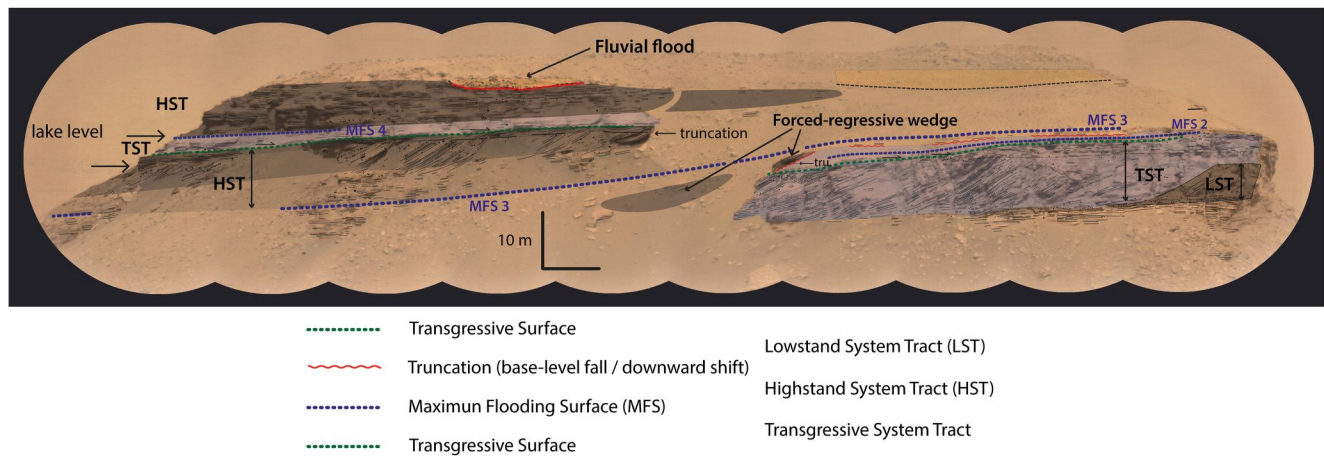


**Figure 9.** Schematic representation of the sequence stratigraphic prisms characterized at Kodiak, with succession of Lowstand, Highstand and Transgressive System Tracts (and associated sequence boundaries) interpreted to reflect successive meter-scale rises and falls of the lake-level through time during and in-between deposition of the different Units/mouth bars of Kodiak butte.

Sigmoidal slope profiles develop when the delta-plain breaks are rounded from erosion and sediment by-pass, or when the delta top plain has already transitioned to subaqueous delta deposition. The lower slope remains exponential and approaches the basin floor asymptotically resulting from the exponential decay of sedimentation.

In addition to those geometries (cf. Figure 8), we observe at Kodiak that the vertical difference between the delta top and the delta toe ranges from approximately 5 to 10 m. The apparent slope inclination values vary from approximately 10 to 35°. Nevertheless, there is no clear correlation between the slope angles, the slope heights, and the types of profiles (Figure 8).

## 5.2. Stratigraphic Architecture

Figure 8 highlights that the set of inclined and horizontal beds that make up Units 0 to 2 are divided into several stratal packages composed of discrete bundles of geometrically similar beds bounded by unconformities. These unconformities are referred to as sequence boundaries (black lines in Figure 8). Sequence boundaries are surfaces of stratal discontinuity and their correlative conformity. Four types of geometries of accretionary sub-units that correspond to individual depositional sequences can be distinguished through the deltaic units of Kodiak, in agreement with the types of slope curvature previously identified: linear wedge, exponential wedge, asymmetrical sigmoid, and symmetrical sigmoid.

The linear and exponential wedge types are accretionary units that do not show any continuity of the foresets with the distal delta plain deposits (i.e., topsets). These commonly have internal toplap (i.e., upper truncation of initially inclined strata), and display either a linear, straight, or an exponential slope profile (e.g., red sub-units in Figure 8). Asymmetrical sigmoid accretionary units are characterized by thicker slope deposits than delta plain deposits and distal thinning-out of the foresets (cf. toesets; e.g., orange sub-units in Figure 8). In symmetrical sigmoid accretionary units, the thickness difference between the slope and delta plain deposits is less than in the asymmetrical sigmoid accretionary unit since bounding surfaces both above and below inclined bedding are almost parallel, except where the inclined foreset beds thins-out into the distal toesets (e.g., green sub-unit in Figure 8b).

Periods of progradation (P), that is, lateral accretion of the foresets correlative of horizontal lakeward migration of the shoreline, are manifested by asymmetrical accretionary units (sigmoid, linear, exponential), and conspicuous truncations of the upper parts of foresets by the topsets, resulting from lateral migration of the shoreline. The asymmetrical wedge morphologies indicate sediments were transported to the delta front and weak to no preservation of the delta plain deposits. Conversely, periods of aggradation (A), that is, vertical stratal stacking on the delta plain and upward migration trend of the delta shoreline, are characterized by symmetrical sigmoid accretionary units, with some preservation of the delta plain deposits.

**Table 2**

*Sequence Stratigraphy Chain of Lake-Level Variations Observed at Kodiak, and Their Representative (Sub-)Units at the Outcrop*

Supra-order lake-level cycles	Lake-levels	Remarkable stratigraphic surfaces		Systems tracts	Units	
			Disconformity		Boulder unit	Sub-units
Cycle 4	Highstand			Highstand ST	U2	U2.1-U2.2
	High	MFS 4	Conformity			
	Rise			Transgressive ST		Unnamed
Cycle 3		Transgressive Surface	Paraconformity			
	Highstand			Highstand ST		Unnamed
	High	MFS 3	Conformity			
	Rise			Transgressive ST	Unnamed	
Cycle 2		Transgressive Surface	Paraconformity			
	Lowstand			Forced-regressive wedge	U1.bis	
	Fall	Downward shift Surface	Angular conformity		Truncation surface	
	Highstand			Highstand ST	Unnamed	
	High	MFS2	Conformity			
				Transgressive ST	Unnamed	
Cycle 1		First Flooding Surface	Disconformity		Ravinement surface	
	Rise				U1	U1.2-U1.7
		Transgressive Surface	Paraconformity			
	Lowstand			Lowstand ST		U1.1
	Fall	Downward shift Surface	Angular conformity		Unidentified	
	Highstand			Highstand ST	U0	U0.1-U0.2
	High	MFS1	Conformity		Unidentified	

Note. ST: System Tracts.

At Kodiak, we observe that most of the deltaic deposition occurred via progradation, with units displaying a strictly progradational character (sub-units 0.1, 1.1, 1.5, 1.7, 2.1, and 2.2, Figure 8) and a mixed progradational-aggradational pattern (although more commonly progradational; sub-units 1.2, 1.3, 1.4, 1.6, 1bis, Figure 8). The only primarily aggradational pattern observed occurred at the time of sub-unit 0.2 deposition (Figure 8b).

### 5.3. Identification of Hydrogeologic Cycles and Lake-Level Changes

The progradational versus aggradational accretional pattern of the Kodiak butte sequences ultimately reflects a volumetric partitioning of sediments between the delta plain and delta slope. Sediment volume partitioning is a consequence of both the dynamic changes in accommodation in different depositional environments that occur with changes of the base-level (Cross, 1988), as well as the geographic variation of accommodation. For example, accommodation in the delta plain and upper delta slope is created in more landward positions during lake-level rise (e.g., Bardaji et al., 1990; Longhitano, 2008; Rohais et al., 2008; Somoza et al., 1998). This is accompanied by an increase in the volume of sediments that accumulate in non-lacustrine facies tracts, with less sediment transported to and accumulated in the lake. By contrast, accommodation decreases inland during lake-level fall, with more sediment bypassed lakeward, and the volume of sediment partitioned into the delta slope increases (e.g., Bardaji et al., 1990; Longhitano, 2008; Rohais et al., 2008; Somoza et al., 1998). In Jezero crater, we can identify two scales of changes in accommodation, hence of the lake-level, both within (higher-order) and between (lower-order) successive sequences.

Within individual units, we identify relative lake-level changes that occurred during the deposition of a single mouth bar, notably leading to the migration of the shoreline (cf. Figure 8). Two individual depositional sequences can be depicted through Unit 0, seven through Unit 1, and two through Unit 2 (Figure 8). Unit 0 shows a purely prograding system (U0.1) overlain by a mixed prograding and aggrading system (U0.2; Figure 8b). Unit 1 is

marked by an uneven succession of purely prograding systems (U1.1, U1.5, U1.7) interrupted by prograding - aggrading ones (U1.2 to U1.4, U1.6; Figures 8a and 8b). Unit 2 is characterized by purely prograding systems (U2.1 and U2.2; Figure 8a). In the absence of tectonically created accommodation, these observations provide evidence that the prograding and aggrading accretionary sub-units likely respond to contemporaneous lake-level rises, while purely prograding wedges point to invariant lake-levels. Shifts between similar wedges reflect the shift of the main direction of the delta slope construction without any change in the lake-level (as evidenced within Unit 1, Figure 8).

The geometry observed in sub-units U2.1 and U2.2 (Figure 8a), which show horizontal topset beds progressively incising planar foreset beds, exemplify the fact that delta slope prograded here in concert with a stable level of the lake. This suggests that lake-level fluctuates at the scale of Kodiak's sub-units, independent of potential fluctuations of the water flow that enters the lake at Kodiak. Otherwise, we would expect to see more rounded, sigmoid accretionary deposits at the outer edge of the delta plain. The magnitude of these higher-order lake-level fluctuations can be evaluated to be on the order of a couple of meters, based on the vertical thickness of the aggrading part of the wedges.

Larger-scale changes in accommodation within Jezero crater are then recorded at the scale of the three main stratigraphic units observed in Kodiak butte, and highlight lower-order changes occurring between and leading to the formation of individual mouth bars. The northern face of Kodiak clearly exposes the geometric relationship between Units 0 and 1 (e.g., Figure 8b). The most striking feature that can be observed is that the flat top surface of the lowermost sub-unit of Unit 1, that is, U1.1, is situated at an elevation a few meters below its counterpart of the uppermost sub-unit of Unit 0, that is, U0.1. The elevation difference of those surfaces (~5 m), which are inferred to represent the delta shoreline, implies that lake-level dropped after the emplacement of Unit 0 and that the lowermost sub-unit U1.1 of Unit U1 represents a Lowstand Systems Tract (Figure 9, Table 2).

The eastern face of Kodiak shows that the upper part of Unit 1 is substantially degraded at its southern edge with a lakeward down-stepping surface that cuts the topsets beds of the unit (Figures 8a and 9). This surface is here interpreted to be a ravinement surface, which represents an erosive surface resulting from the action of waves as the shoreline retreated landward in response to a concomitant lake-level rise and the local shutdown of sediment deposition. Accordingly, the recessive interval marking sediments onlapping the surface is interpreted as a transgressive system tract built by the deposits that accumulated there until the time of maximum transgression (i.e., lake-level rise; Figure 9, Table 2).

The lower part of the large recessive interval that separates Unit 1 from Unit 2 records a resistant wedge a few meters in thickness that comprises foreset strata (sub-unit U1.bis; Figures 8a and 9). The foresets clearly truncate the underlying horizontal topset beds, suggesting that the wedge is a slope-perched delta deposited at the mouth of a potential incision into the delta top after decreasing accommodation on the upper slope during the lake-level fall. In sequence stratigraphic terms, this feature represents a forced-regressive wedge (Figure 9, Table 2).

The largest part of the recessive interval between Unit 1 and Unit 2 is mostly covered, and thus is postulated to be composed of thinly bedded, fine-grained deposits. It is speculated to represent a combination of a transgressive systems tract, a maximum flooding surface, and an early highstand wedge (Figure 9, Table 2), all of which are expected to be represented by generally fine-grained strata that are poorly preserved in Kodiak butte. By contrast, the lower part of the Unit 2 cliff is composed of the more coarsely grained progradational foresets of sub-units U2.1 and U2.2 (Figure 8a), that best corresponds to a late highstand systems tract. The aggradational pattern of beds shown by the upper half of U2.2 is speculated to mark the shift to an additional cycle of lake-level rise (Figure 9, Table 2).

In summary, Kodiak butte exhibits four low-order depositional cycles (Figure 9; Table 2). Cycles 3 and 4 are composed of Transgressive and Highstand Systems Tracts only, while Cycles 1 and 2 contain clear lowstand wedges. The cycles are interpreted to be related to changes in accommodation through time in the delta plain and upper slope regions. Transgressive Systems Tracts express the creation of accommodation, with Maximum Flooding Surfaces (MFS) representing the highest accommodation for each cycle. Highstand Systems Tracts represent a decrease to invariance in the accommodation creation. Downward Shift surfaces and associated Lowstand wedges reflect removal of accommodation (minor for the forced-regressive wedge U1.bis of Cycle 2). Creation of accommodation is related to absolute lake-level rises in the absence of substantial subsidence of the thick Martian crust, since sediment compaction is here a negligible process. Loss of accommodation is related to



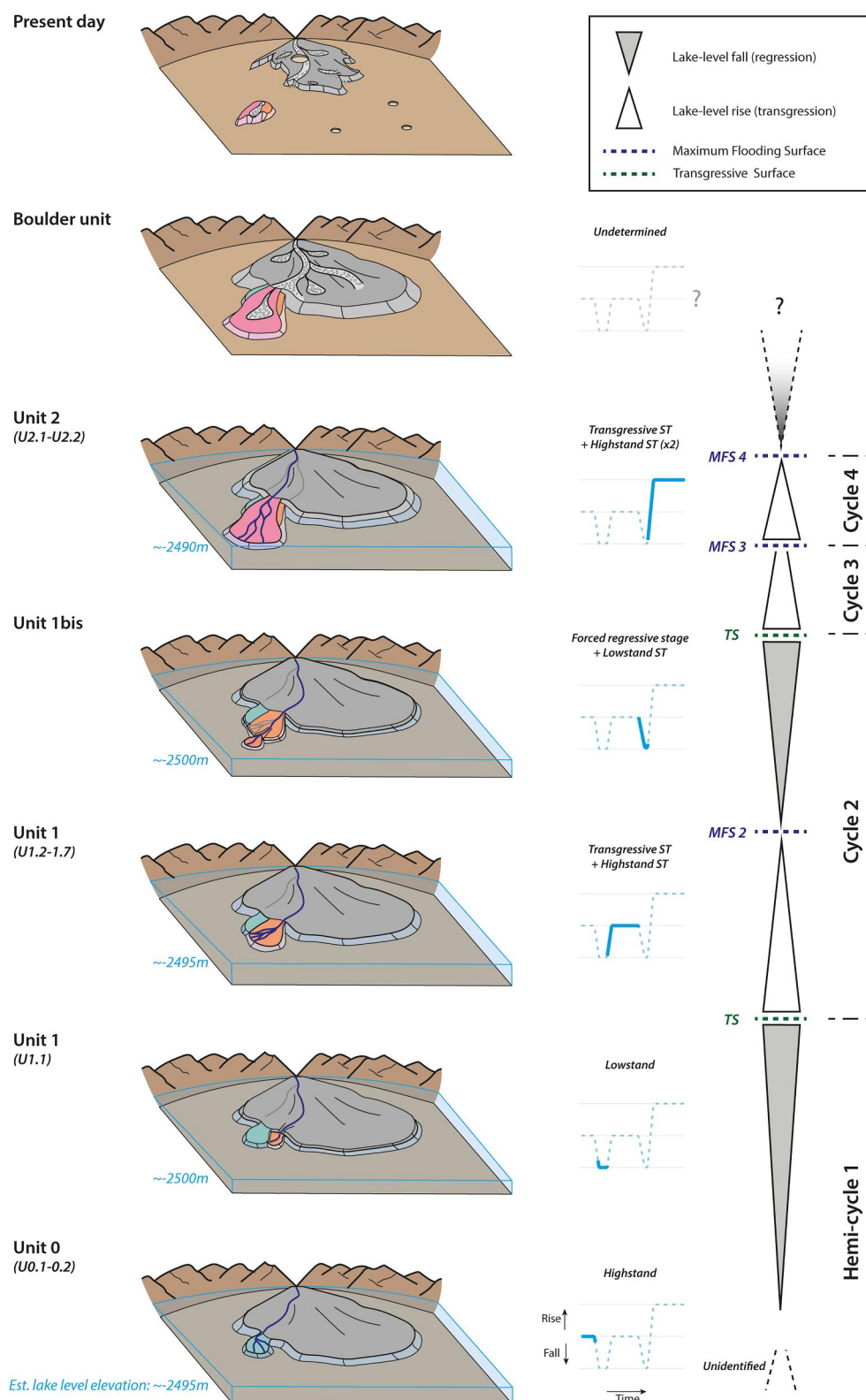


**Figure 10.** Proposed synthetic model (not to scale) of deposition of the different deltaic mouth bars (Units 0 to 2) controlled by lake-level fluctuations, highlighting 4 hydrogeologic cycles occurring in Jezero crater lake at the time of Kodiak deposition. The stage of deposition of the Boulder unit is not timely constrained and is interpreted as being disconnected from the main deltaic phase. The present-day stage is also illustrated highlighting the erosion-driven isolation of the Kodiak butte from the main delta.

absolute lake-level falls since there is no alternative credible way of cutting deposits of the delta plain edge (U1. bis) or drawing down the lake shoreline level (U1.1). The overall magnitude of these low-order lake-level fluctuations is on the order of 5–10 m (between  $-2,500$  and  $-2,490$  m).

## 6. Implications for Jezero Lake Evolution

### 6.1. 4D Evolution of the Delta System at Kodiak

Figure 10 shows a model developed to illustrate the proposed evolution of the western Jezero delta at the time of Kodiak deposition, its build-up resulting from the emplacement of amalgamated deltaic mouth bars in relation to successive rises and falls of the lake-level of a magnitude of a few meters ( $\sim 5$ – $10$  m, Figure 10). Lake level elevation is estimated by mapping the elevation of the transition between foresets and topsets as a proxy to accurately identify and map the paleo-shoreline for each stratigraphic cycle (1–4, cf. Table 2 and Figure 9) identified across Units 0 to 2.

The first episode of lake-level rise and fall that we document at Kodiak is identified as a partial expression of Cycle 1. While we do not observe the record of the lake-level rise, Unit 0 was deposited during a period of highstand, with the contemporaneous lake-level estimated to be at  $\sim -2,495$  m (in present-day elevation; Figure 10). After this period of stable lake-level allowing for the progradation of Unit 0, we observe a lake-level fall. This led to the formation of a new mouth bar starting with the emplacement of sub-unit 1.1, characterizing a lowstand during which the lake-level is estimated to be circa  $-2,500$  m (Figure 10).

Cycle 2 is represented by the rest of Unit 1 (sub-units 1.2 to 1.7 and 1bis, Figure 10), and is the only example of a complete depositional cycle recorded at Kodiak. Lake-level rise and stabilization at an elevation of approximately  $-2,495$  m is represented by progradational sub-units 1.2 to 1.7 that were emplaced laterally and against the previous deposits of Unit 0. After a period of lake-level highstand, the lake-level fell again, resulting in a local erosional unconformity at the top of sub-units 1.6 and 1.7, and emplacement of a forced-regression lowstand package of sub-unit 1bis. Lake level at the time of this forced regression was again circa  $-2,500$  m.

Finally, Cycles 3 and 4 are incomplete and their records across Unit 2 are amalgamated; they represent a rise and a stabilization of the lake-level at an elevation of approximately  $-2,490$  m (the highest lake-level recorded at Kodiak), which allowed the continuous progradation (and aggradation) of Unit 2 on top of previous Units 0 and 1 as highstand deposits (Figure 10).

The latest sedimentary activity recorded at Kodiak led to the emplacement of the non-deltaic bouldery unit, likely through episodic intense floods (e.g., Mangold et al., 2021; Mangold et al., 2024). However, we cannot determine with precision whether these events occurred recently after Cycle 4 or several tens, hundreds, or thousands of years after, if not more. Also, it is not possible to know whether a lake was still in place in the Jezero crater at the time these chaotic clast-supported boulder conglomerates were deposited (Figure 10).

### 6.2. Factors Controlling Lake-Level Fluctuations

Kodiak's stratigraphic record shows the deposition of successive individual deltaic mouth bars through time. These bars were emplaced as a response to changes in local accommodation, controlled by rises and falls of the lake-level. By considering the elevation range of this deltaic bar complex, we conclude that Kodiak butte was built when Jezero lake was a closed-basin system (cf. Mangold et al., 2021). As such, changes in lake-level may have been controlled by variations in the water supply driven by several intrinsic or extrinsic factors including: high intensity rainfall episodes (flash floods) and snow melts (either seasonal, impact-driven or related to volcanic episodes), breaches of upstream lake dams, and losses due to evaporation or infiltration to the regional ground water table. We suggest that the lower-order unit scale lake-level variations (i.e., emplacement of deltaic mouth bars) were likely controlled by climatic or seasonal-scale phenomena, while smaller-scale fluctuations at the higher-order sub-unit scale (i.e., changes *within* the bars and shoreline migrations) could result from temporally restricted events such as floods or surges in fluvial inputs. Notably, we exclude the possibility of lake-level variation induced by emplacement of an ice-sheet cover (e.g., Yin, 2021), as no characteristic evidence pointing toward a sub-glacial deltaic deposition has been observed, such as moraines or fluid-pressure deformation/fracturation (e.g., Ravier & Buoncristiani, 2018). Rather, recognition of a hierarchy of magnitude within cyclicity observed at Kodiak butte suggest the intriguing possibility of astronomical control, similar to that observed on Earth (e.g., Bardaji et al., 1990; Longhitano, 2008; Rohais et al., 2008; Somoza et al., 1998).

## 7. Conclusions

Detailed observations of Kodiak butte, a distal remnant of the western Jezero delta, were carried out using high-resolution 2D and 3D data acquired as the rover traversed the Jezero crater floor. These observations enable us to characterize three individual stratigraphic Units 0 to 2 on the eastern and northern faces of the butte. These units reveal the characteristic bottomset, toeset, foreset, and topset architecture of a Gilbert-type delta.

We characterized the Kodiak succession into 11 facies grouped into 5 facies associations that represent deposition within a prograding Gilbert-delta, and later (unconformable) deposition from high-energy floods (Mangold et al., 2021, 2024). Each Unit shows similar vertical stacking pattern recording prodeltaic-lacustrine bottomset beds, delta slope toeset and foreset beds, and fluvially influenced topset beds of a braided delta plain.

Using these elements, we have been able to construct a 4D sequence stratigraphic framework detailing the temporal fluctuation of the lake-level across four hydrogeological cycles representing lake-level changes on the order of 5–10 m. These fluctuations are attributed to local variations in water input, which are in turn related to larger-scale climatic events. This suggests that the Jezero delta records a hierarchy of lake-level changes analogous to those on Earth, which could reflect astronomically driven climatic changes.

## Data Availability Statement

All of the Mastcam-Z (Bell & Maki, 2021) images used in this manuscript are freely available through the Planetary Data System Cartography and Imaging Sciences Node. All of the SuperCam's Remote-Micro Imager (Wiens & Maurice, 2021) images used in this manuscript are freely available through the Planetary Data System Geosciences node. Detailed list of used mosaics and their Sol of acquisition is available in Table S2 in Supporting Information S1. All 3D Digital Outcrop Models presented in this manuscript are freely accessible for visualization, including in Virtual Reality, on the Sketchfab web-platform (<https://sketchfab.com/LPG-3D> and <https://sketchfab.com/Mastcam-Z>). Supplementary illustrations and table presented in the Supporting Information S1 of this work are available in the Zenodo open-source online repository (Caravaca et al., 2023).

## Acknowledgments

The authors are thankful to the engineering and science teams of the Mars 2020 mission for carrying out operations that allowed acquisition of the data presented in this work. We also thank Deanne Rogers (Editor), Janok P. Bhattacharya and another anonymous Reviewer for their comments and suggestions that helped improve this manuscript. GC, GD, NM, SLM, OG, OB, and SM work was supported by French Space Agency CNES, focused on SuperCam and on Mars2020-Perseverance. SG acknowledges support from the UK Space Agency under Grants ST/X002373/1 and ST/Y000153/1. LCK and RMEW acknowledge support from the M2020 SHERLOC-WATSON instrument team. CT, JFB, JIN and JWR acknowledge support from the M2020 Mastcam-Z instrument team. AJW acknowledges support from the M2020 Participating Scientist program under Grant 80NSSC21K0332. KMS's effort was carried out at the Jet Propulsion Laboratory, California Institute of Technology under a contract with the National Aeronautics and Space Administration. RCW acknowledges support from the National Aeronautics and Space Administration under Grant F.10050029.02.003.

## References

- Adams, E. W. (2001). Subaquatic slope curvature and its relation to sedimentary processes and sediment composition. (PhD thesis). Faculteit der Aardwetenschappen Vrije Universiteit.
- Adler, J. B., Bell, J. F., Fawdon, P., Davis, J., Warner, N. H., Sefton-Nash, E., & Harrison, T. N. (2019). Hypotheses for the origin of the Hypanis fan-shaped deposit at the edge of the Chryse escarpment, Mars: Is it a delta? *Icarus*, 319, 885–908. <https://doi.org/10.1016/j.icarus.2018.05.021>
- Agisoft Metashape Professional. (2023). *Agisoft Metashape Professional (version 1.8.5)*. Agisoft LLC. Retrieved from <https://www.agisoft.com/>
- Allen, J. R. L. (1982). *Sedimentary structures: Their character and physical basis* (Vol. 30A). Elsevier.
- Ansan, V., Loizeau, D., Mangold, N., Le Mouélic, S., Carter, J., Poulet, F., et al. (2011). Stratigraphy, mineralogy, and origin of layered deposits inside Terby crater, Mars. *Icarus*, 211(1), 273–304. <https://doi.org/10.1016/j.icarus.2010.09.011>
- Arvidson, R. E., & Catalano, J. G. (2018). Chapter 4—Martian habitability as inferred from landed mission observations. In N. A. Cabrol & E. A. Grin (Eds.), *From habitability to life on Mars* (pp. 77–126). Elsevier. <https://doi.org/10.1016/B978-0-12-809935-3.00004-9>
- Banham, S. G., Gupta, S., Rubin, D. M., Bedford, C. C., Edgar, L. A., Bryk, A. B., et al. (2022). Evidence for fluctuating wind in shaping an ancient Martian dune field: The stinson formation at the Greenheugh Pediment, Gale Crater. *Journal of Geophysical Research: Planets*, 127(9), e2021JE007023. <https://doi.org/10.1029/2021JE007023>
- Bardaji, T., Dabrio, C. J., Goy, J. L., Somoza, L., & Zazo, C. (1990). Pleistocene fan deltas in southeastern Iberian Peninsula: Sedimentary controls and sea-level changes. In A. Colella & D. B. Prior (Eds.), *Coarse-grained deltas* (1st ed., pp. 129–151). Wiley. <https://doi.org/10.1002/9781444303858.ch7>
- Barnes, R., Gupta, S., Traxler, C., Ortner, T., Bauer, A., Hesina, G., et al. (2018). Geological analysis of Martian rover-derived digital outcrop models using the 3-D visualization tool, planetary robotics 3-D viewer—PRO3D. *Earth and Space Science*, 5(7), 285–307. <https://doi.org/10.1002/2018EA000374>
- Bell, J. F., & Maki, J. M. (2021). Mars 2020 mast camera zoom bundle, from operations team, mosaic products [Dataset]. *PDS*. <https://doi.org/10.17189/BMKQ-NM72>
- Bell, J. F., Maki, J. N., Mehall, G. L., Ravine, M. A., Caplinger, M. A., Bailey, Z. J., et al. (2021). The Mars 2020 perseverance rover mast camera zoom (Mastcam-Z) multispectral, stereoscopic imaging investigation. *Space Science Reviews*, 217(1), 24. <https://doi.org/10.1007/s11214-020-00755-x>
- Breda, A., Mellere, D., Massari, F., & Asioli, A. (2009). Vertically stacked Gilbert-type deltas of Ventimiglia (NW Italy): The Pliocene record of an overfilled Messinian incised valley. *Sedimentary Geology*, 219(1–4), 58–76. <https://doi.org/10.1016/j.sedgeo.2009.04.010>
- Burr, D. M., Williams, R. M. E., Wendell, K. D., Chojnacki, M., & Emery, J. P. (2010). Inverted fluvial features in the Aeolis/Zephyria Plana region, Mars: Formation mechanism and initial paleodischarge estimates. *Journal of Geophysical Research*, 115(E7), E07011. <https://doi.org/10.1029/2009JE003496>
- Caravaca, G., Dromart, G., Mangold, N., Gupta, S., Kah, L., Tate, C., et al. (2023). Supplemental data from: “depositional facies and sequence stratigraphy of Kodiak butte, western delta of Jezero crater, Mars” [Dataset]. *Zenodo*. <https://doi.org/10.5281/ZENODO.10103217>
- Caravaca, G., Le Mouélic, S., Mangold, N., L'Haridon, J., Le Deit, L., & Massé, M. (2020). 3D digital outcrop model reconstruction of the Kimberley outcrop (Gale crater, Mars) and its integration into Virtual Reality for simulated geological analysis. *Planetary and Space Science*, 182, 104808. <https://doi.org/10.1016/j.pss.2019.104808>

- Caravaca, G., Le Mouélic, S., Rapin, W., Dromart, G., Gasnault, O., Fau, A., et al. (2021). Long-distance 3D reconstructions using photogrammetry with Curiosity's ChemCam remote micro-imager in Gale crater (Mars). *Remote Sensing*, 13(20), 4068. <https://doi.org/10.3390/rs13204068>
- Caravaca, G., Mangold, N., Dehouck, E., Schieber, J., Zaugg, L., Bryk, A. B., et al. (2022). From lake to river: Documenting an environmental transition across the Jura/Knockfarril hill members boundary in the Glen Torridon region of Gale crater (Mars). *Journal of Geophysical Research: Planets*, 127(9), e2021JE007093. <https://doi.org/10.1029/2021JE007093>
- Carr, M. H. (2012). The fluvial history of Mars. *Philosophical Transactions of the Royal Society A: Mathematical, Physical & Engineering Sciences*, 370(1666), 2193–2215. <https://doi.org/10.1098/rsta.2011.0500>
- Carter, J., Poulet, F., Bibring, J.-P., Mangold, N., & Murchie, S. (2013). Hydrous minerals on Mars as seen by the CRISM and OMEGA imaging spectrometers: Updated global view. *Journal of Geophysical Research: Planets*, 118(4), 831–858. <https://doi.org/10.1029/2012JE004145>
- Chavarrías, V., Blom, A., Orrú, C., Martín-Vide, J. P., & Viparelli, E. (2018). A sand-gravel Gilbert delta subject to base level change. *Journal of Geophysical Research: Earth Surface*, 123(5), 1160–1179. <https://doi.org/10.1029/2017JF004428>
- Clauzon, G., Le Strat, P., Duvail, C., Do Couto, D., Suc, J.-P., Molliex, S., et al. (2015). The Roussillon basin (S. France): A case-study to distinguish local and regional events between 6 and 3 Ma. *Marine and Petroleum Geology*, 66, 18–40. <https://doi.org/10.1016/j.marpetgeo.2015.03.012>
- Clift, P. D., Olson, E. D., Lechnowskyj, A., Moran, M. G., Barbato, A., & Lorenzo, J. M. (2019). Grain-size variability within a mega-scale point-bar system, False River, Louisiana. *Sedimentology*, 66(2), 408–434. <https://doi.org/10.1111/sed.12528>
- Cross, T. A. (1988). Controls on coal distribution in transgressive-regressive cycles, upper cretaceous, western interior, U.S.A. Retrieved from [https://archives.datapages.com/data/sepm\\_sp/SP42/Controls\\_on\\_Coal\\_Distribution\\_in\\_Transgressive-Regressive\\_Cycles.htm](https://archives.datapages.com/data/sepm_sp/SP42/Controls_on_Coal_Distribution_in_Transgressive-Regressive_Cycles.htm)
- Dabrio, C. J. (1990). Fan-delta facies associations in late neogene and quaternary basins of southeastern Spain. In A. Colella & D. B. Prior (Eds.), *Coarse-grained deltas* (1st ed., pp. 91–111). Wiley. <https://doi.org/10.1002/9781444303858.ch5>
- De Toffoli, B., Plesa, A.-C., Hauber, E., & Breuer, D. (2021). Delta deposits on Mars: A global perspective. *Geophysical Research Letters*, 48(17), e2021GL094271. <https://doi.org/10.1029/2021GL094271>
- Di Achille, G., & Hynek, B. M. (2010). Ancient Ocean on Mars supported by global distribution of deltas and valleys. *Nature Geoscience*, 3(7), 459–463. <https://doi.org/10.1038/ngeo891>
- Dromart, G., Quantin, C., & Broucke, O. (2007). Stratigraphic architectures spotted in southern Melas Chasma, Valles Marineris, Mars. *Geology*, 35(4), 363. <https://doi.org/10.1130/G23350A.1>
- Edgett, K. S., & Sarkar, R. (2021). Recognition of sedimentary rock occurrences in satellite and aerial images of other worlds—Insights from Mars. *Remote Sensing*, 13(21), 4296. <https://doi.org/10.3390/rs13214296>
- Ehlmann, B. L., Mustard, J. F., Murchie, S. L., Bibring, J.-P., Meunier, A., Fraeman, A. A., & Langevin, Y. (2011). Subsurface water and clay mineral formation during the early history of Mars. *Nature*, 479(7371), 53–60. <https://doi.org/10.1038/nature10582>
- Ehlmann, B. L., Mustard, J. F., Murchie, S. L., Poulet, F., Bishop, J. L., Brown, A. J., et al. (2008). Orbital identification of carbonate-bearing rocks on Mars. *Science*, 322(5909), 1828–1832. <https://doi.org/10.1126/science.1164759>
- Farley, K. A., Williford, K. H., Stack, K. M., Bhartia, R., Chen, A., de la Torre, M., et al. (2020). Mars 2020 mission overview. *Space Science Reviews*, 216(8), 142. <https://doi.org/10.1007/s11214-020-00762-y>
- Fassett, C. I., & Head, J. W. (2005). Fluvial sedimentary deposits on Mars: Ancient deltas in a crater lake in the Nili Fossae region: Fluvial sedimentary deposits on Mars. *Geophysical Research Letters*, 32(14), L14201. <https://doi.org/10.1029/2005GL023456>
- Fayol, H. (1886). Résumé de la théorie des deltas et histoire de la formation du Bassin de Commeny. *Bulletin de la Société Géologique de France*, 16, 968–978.
- Gasnault, O., Virmontois, C., Maurice, S., Wiens, R. C., Le Mouélic, S., Bernardi, P., et al. (2021). What SuperCam will see: The remote micro-imager aboard perseverance. In *52nd lunar and planetary science conference*. Retrieved from <https://hal.science/hal-03453205/>
- Ghinassi, M., Ielpi, A., Aldinucci, M., & Fustic, M. (2016). Downstream-migrating fluvial point bars in the rock record. *Sedimentary Geology*, 334, 66–96. <https://doi.org/10.1016/j.sedgeo.2016.01.005>
- Ghinassi, M., Nemec, W., Aldinucci, M., Nehyba, S., Özaksoy, V., & Fidolini, F. (2014). Plan-form evolution of ancient meandering rivers reconstructed from longitudinal outcrop sections. *Sedimentology*, 61(4), 952–977. <https://doi.org/10.1111/sed.12081>
- Gilbert, G. K. (1885). The topographic features of lake shores (annual report of the US Geological Survey No. 5) (pp. 69–123).
- Gobo, K., Ghinassi, M., & Nemec, W. (2014). Reciprocal changes in foreset to bottomset facies in a Gilbert-type delta: Response to short-term changes in base level. *Journal of Sedimentary Research*, 84(11), 1079–1095. <https://doi.org/10.2110/jsr.2014.83>
- Gobo, K., Ghinassi, M., & Nemec, W. (2015). Gilbert-type deltas recording short-term base-level changes: Delta-brink morphodynamics and related foreset facies. *Sedimentology*, 62(7), 1923–1949. <https://doi.org/10.1111/sed.12212>
- Goudge, T. A., Milliken, R. E., Head, J. W., Mustard, J. F., & Fassett, C. I. (2017). Sedimentological evidence for a deltaic origin of the western fan deposit in Jezero crater, Mars and implications for future exploration. *Earth and Planetary Science Letters*, 458, 357–365. <https://doi.org/10.1016/j.epsl.2016.10.056>
- Goudge, T. A., Mohrig, D., Cardenas, B. T., Hughes, C. M., & Fassett, C. I. (2018). Stratigraphy and paleohydrology of delta channel deposits, Jezero crater, Mars. *Icarus*, 301, 58–75. <https://doi.org/10.1016/j.icarus.2017.09.034>
- Goudge, T. A., Mustard, J. F., Head, J. W., Fassett, C. I., & Wiseman, S. M. (2015). Assessing the mineralogy of the watershed and fan deposits of the Jezero crater paleolake system, Mars. *Journal of Geophysical Research: Planets*, 120(4), 775–808. <https://doi.org/10.1002/2014JE004782>
- Grotzinger, J. P., Gupta, S., Malin, M. C., Rubin, D. M., Schieber, J., Siebach, K., et al. (2015). Deposition, exhumation, and paleoclimate of an ancient lake deposit, Gale crater, Mars. *Science*, 350(6257), aac7575. <https://doi.org/10.1126/science.aac7575>
- Grotzinger, J. P., Hayes, A. G., Lamb, M. P., & McLennan, S. M. (2013). Sedimentary processes on Earth, Mars, Titan, and Venus. In *Comparative climatology of terrestrial planets*. University of Arizona Press. [https://doi.org/10.2458/azu\\_uapress.9780816530595-ch18](https://doi.org/10.2458/azu_uapress.9780816530595-ch18)
- Gupta, S., Bell, J. F., Caravaca, G., Kanine, O. A., Mangold, N., Stack, K., et al. (2022). Fine-scale sedimentary architecture of the Jezero western delta front. In *AGU fall meeting 2022* (Vol. 2022, p. P56A-05). Retrieved from <https://ui.adsabs.harvard.edu/abs/2022AGUFM.P56A.05G>
- Horgan, B. H. N., Anderson, R. B., Dromart, G., Amador, E. S., & Rice, M. S. (2020). The mineral diversity of Jezero crater: Evidence for possible lacustrine carbonates on Mars. *Icarus*, 339, 113526. <https://doi.org/10.1016/j.icarus.2019.113526>
- Hynek, B. M., Beach, M., & Hoke, M. R. T. (2010). Updated global map of Martian valley networks and implications for climate and hydrologic processes. *Journal of Geophysical Research*, 115(E9), E09008. <https://doi.org/10.1029/2009JE003548>
- Jones, R., Marcelissen, R., & Fralick, P. (2022). Sedimentology and stratigraphy of a large, pre-vegetation deltaic complex. *Frontiers in Earth Science*, 10, 875838. <https://doi.org/10.3389/feart.2022.875838>
- Kargel, J. S. (2004). *Mars: A warmer, wetter planet*. Springer.



- Knox, R. L. (2013). Changes in recent effective discharge and geomorphology near the old river control on the lower Mississippi River. (MSc thesis). University of Texas. Retrieved from <https://repositories.lib.utexas.edu/bitstream/handle/2152/21806/KNOX-THESIS-2013.pdf?sequence=1>
- Kronyak, R. E., Stack, K. M., Sholes, S. F., Sun, V. Z., Supta, S., Shuster, D. L., & Caravaca, G. (2023). Geomorphology and relative ages of channel belt deposits in Jezero's western delta. In *54th lunar and planetary science conference (LPSC 2023)*. The Woodlands, TX, USA. Retrieved from <https://www.hou.usra.edu/meetings/lpsc2023/pdf/2067.pdf>
- Lazar, O. R., Bohacs, K. M., Macquaker, J. H. S., Schieber, J., & Demko, T. M. (2015). Capturing key attributes of fine-grained sedimentary rocks in outcrops, cores, and thin sections: Nomenclature and description guidelines. *Journal of Sedimentary Research*, 85(3), 230–246. <https://doi.org/10.2110/jsr.2015.11>
- Le Mouélic, S., Enguehard, P., Schmitt, H. H., Caravaca, G., Seignovet, B., Mangold, N., et al. (2020). Investigating lunar boulders at the Apollo 17 landing site using photogrammetry and virtual reality. *Remote Sensing*, 12(11), 1900. <https://doi.org/10.3390/rs12111900>
- Le Mouélic, S., L'Haridon, J., Civet, F., Mangold, N., Triantafyllou, A., Massé, M., et al. (2018). Using virtual reality to investigate geological outcrops on planetary surfaces, 13366. Retrieved from <https://ui.adsabs.harvard.edu/abs/2018EGUGA..2013366L>
- Longhitano, S. G. (2008). Sedimentary facies and sequence stratigraphy of coarse-grained Gilbert-type deltas within the Pliocene thrust-top Potenza basin (southern Apennines, Italy). *Sedimentary Geology*, 210(3–4), 87–110. <https://doi.org/10.1016/j.sedgeo.2008.07.004>
- Malin, M. C., & Edgett, K. S. (2000). Sedimentary rocks of early Mars. *Science*, 290(5498), 1927–1937. <https://doi.org/10.1126/science.290.5498.1927>
- Mangold, N., Caravaca, G., Gupta, S., Williams, R. M. E., Dromart, G., Gasnault, O., et al. (2024). Architecture of the fluvial and deltaic deposits of the east of Jezero crater western fan. *Journal of Geophysical Research: Planets*, 129(3), e2023JE008204. <https://doi.org/10.1029/2023je008204>
- Mangold, N., Dromart, G., Ansan, V., Salese, F., Kleinhans, M. G., Massé, M., et al. (2020). Fluvial regimes, morphometry, and age of Jezero Crater Paleolake inlet valleys and their exobiological significance for the 2020 rover mission landing site. *Astrobiology*, 20(8), 994–1013. <https://doi.org/10.1089/ast.2019.2132>
- Mangold, N., Gupta, S., Gasnault, O., Dromart, G., Tarnas, J. D., Sholes, S. F., et al. (2021). Perseverance rover reveals an ancient delta-lake system and flood deposits at Jezero crater, Mars. *Science*, 374(6568), 711–717. <https://doi.org/10.1126/science.abc4051>
- Mangold, N., Kite, E. S., Kleinhans, M. G., Newsom, H., Ansan, V., Hauber, E., et al. (2012). The origin and timing of fluvial activity at Eberswalde crater, Mars. *Icarus*, 220(2), 530–551. <https://doi.org/10.1016/j.icarus.2012.05.026>
- Massari, F. (1996). Upper-flow-regime stratification types on steep-face, coarse-grained, Gilbert-type progradational wedges (Pleistocene, southern Italy). *SEPM Journal of Sedimentary Research*, 66. <https://doi.org/10.1306/D426834C-2B26-11D7-8648000102C1865D>
- Maurice, S., Wiens, R. C., Bernardi, P., Caïs, P., Robinson, S., Nelson, T., et al. (2021). The SuperCam instrument suite on the Mars 2020 rover: Science objectives and mast-unit description. *Space Science Reviews*, 217(3), 47. <https://doi.org/10.1007/s11214-021-00807-w>
- McEwen, A. S., Eliason, E. M., Bergstrom, J. W., Bridges, N. T., Hansen, C. J., Delamere, W. A., et al. (2007). Mars reconnaissance orbiter's High Resolution Imaging Science Experiment (HiRISE). *Journal of Geophysical Research*, 112(E5), 2005JE002605. <https://doi.org/10.1029/2005JE002605>
- Miall, A. (2014). *Fluvial depositional systems*. Springer International Publishing. <https://doi.org/10.1007/978-3-319-00666-6>
- Mitchum, R. M., Vail, P. R., & Thompson, S. (1977). Seismic stratigraphy and global changes of sea level: Part 2. The depositional sequence as a basic unit for stratigraphic analysis: Section 2. Application of seismic reflection configuration to stratigraphic. *Interpretation*, 165, 53–62. Retrieved from <http://archives.datapages.com/data/specpubs/seismic1/data/a165/a165/0001/0050/0053.htm>
- Morgan, A. M., Wilson, S. A., & Howard, A. D. (2022). The global distribution and morphologic characteristics of fan-shaped sedimentary landforms on Mars. *Icarus*, 385, 115137. <https://doi.org/10.1016/j.icarus.2022.115137>
- Nemec, W. (1990a). Aspects of sediment movement on steep delta slopes. In A. Colella & D. B. Prior (Eds.), *Coarse-grained deltas* (1st ed., pp. 29–73). Wiley. <https://doi.org/10.1002/9781444303858.ch3>
- Nemec, W. (1990b). Deltas—Remarks on terminology and classification. In A. Colella & D. B. Prior (Eds.), *Coarse-grained deltas* (1st ed., pp. 1–12). Wiley. <https://doi.org/10.1002/9781444303858.ch1>
- Nemec, W. (1996). *Principles of lithostratigraphic logging and facies analysis. Short course lecture notes*. University of Bergen
- Nemec, W., & Steel, R. J. (1984). Alluvial and coastal conglomerates: Their significant features and some comments on gravelly mass-flow deposits. (Vol. 1–31). Retrieved from [http://archives.datapages.com/data/cspg\\_sp/data/010/010001/1\\_cspgsp0100001.htm](http://archives.datapages.com/data/cspg_sp/data/010/010001/1_cspgsp0100001.htm)
- Ori, G. G., & Roveri, M. (1987). Geometries of Gilbert-type deltas and large channels in the meteora conglomerate, Meso-Hellenic basin (Oligo-Miocene), central Greece. *Sedimentology*, 34(5), 845–859. <https://doi.org/10.1111/j.1365-3091.1987.tb00808.x>
- Paar, G., Ortner, T., Tate, C., Deen, R. G., Abercrombie, P., Vona, M., et al. (2023). Three-dimensional data preparation and immersive mission-spanning visualization and analysis of Mars 2020 Mastcam-Z stereo image sequences. *Earth and Space Science*, 10(3), e2022EA002532. <https://doi.org/10.1029/2022EA002532>
- Palucis, M. C., Dietrich, W. E., Williams, R. M. E., Hayes, A. G., Parker, T., Sumner, D. Y., et al. (2016). Sequence and relative timing of large lakes in Gale crater (Mars) after the formation of Mount Sharp. *Journal of Geophysical Research: Planets*, 121(3), 472–496. <https://doi.org/10.1002/2015JE004905>
- Postma, G. (1984). Slumps and their deposits in fan delta front and slope. *Geology*, 12(1), 27. [https://doi.org/10.1130/0091-7613\(1984\)12<27:SATDIF>2.0.CO;2](https://doi.org/10.1130/0091-7613(1984)12<27:SATDIF>2.0.CO;2)
- Postma, G. (1986). Classification for sediment gravity-flow deposits based on flow conditions during sedimentation. *Geology*, 14(4), 291. [https://doi.org/10.1130/0091-7613\(1986\)14<291:CFSGDB>2.0.CO;2](https://doi.org/10.1130/0091-7613(1986)14<291:CFSGDB>2.0.CO;2)
- Postma, G. (1990). Depositional architecture and facies of river and fan deltas: A synthesis. In A. Colella & D. B. Prior (Eds.), *Coarse-grained deltas* (1st ed., pp. 13–27). Wiley. <https://doi.org/10.1002/9781444303858.ch2>
- Poulet, F., Bibring, J.-P., Mustard, J. F., Gendrin, A., Mangold, N., Langevin, Y., et al. (2005). Phyllosilicates on Mars and implications for early Martian climate. *Nature*, 438(7068), 623–627. <https://doi.org/10.1038/nature04274>
- Rapin, W., Dromart, G., Rubin, D., Deit, L. L., Mangold, N., Edgar, L. A., et al. (2021). Alternating wet and dry depositional environments recorded in the stratigraphy of Mount Sharp at Gale crater, Mars. *Geology*, 49(7), 842–846. <https://doi.org/10.1130/G48519.1>
- Ravier, E., & Buoncristiani, J.-F. (2018). Glaciohydrogeology. In *Past glacial environments* (pp. 431–466). Elsevier. <https://doi.org/10.1016/B978-0-08-100524-8.00013-0>
- Rohais, S., Eschard, R., & Guillocheau, F. (2008). Depositional model and stratigraphic architecture of rift climax Gilbert-type fan deltas (Gulf of Corinth, Greece). *Sedimentary Geology*, 210(3), 132–145. <https://doi.org/10.1016/j.sedgeo.2008.08.001>
- Rubi, R., Rohais, S., Bourquin, S., Moretti, I., & Desaubliaux, G. (2018). Processes and typology in Gilbert-type delta bottomset deposits based on outcrop examples in the Corinth Rift. *Marine and Petroleum Geology*, 92, 193–212. <https://doi.org/10.1016/j.marpetgeo.2018.02.014>

- Salese, F., Kleinhans, M. G., Mangold, N., Ansan, V., McMahon, W., De Haas, T., & Dromart, G. (2020). Estimated minimum life span of the Jezero fluvial delta (Mars). *Astrobiology*, 20(8), 977–993. <https://doi.org/10.1089/ast.2020.2228>
- Schlager, W. (1993). Accommodation and supply—A dual control on stratigraphic sequences. *Sedimentary Geology*, 86(1–2), 111–136. [https://doi.org/10.1016/0037-0738\(93\)90136-S](https://doi.org/10.1016/0037-0738(93)90136-S)
- Schon, S. C., Head, J. W., & Fassett, C. I. (2012). An overfilled lacustrine system and progradational delta in Jezero crater, Mars: Implications for Noachian climate. *Planetary and Space Science*, 67(1), 28–45. <https://doi.org/10.1016/j.pss.2012.02.003>
- Somoza, L., Barnolas, A., Arasa, A., Maestro, A., Rees, J. G., & Hernandez-Molina, F. J. (1998). Architectural stacking patterns of the Ebro delta controlled by Holocene high-frequency eustatic fluctuations, delta-lobe switching and subsidence processes. *Sedimentary Geology*, 117(1–2), 11–32. [https://doi.org/10.1016/S0037-0738\(97\)00121-8](https://doi.org/10.1016/S0037-0738(97)00121-8)
- Stack, K. M., Williams, N. R., Calef, F., Sun, V. Z., Williford, K. H., Farley, K. A., et al. (2020). Photogeologic map of the perseverance rover field site in Jezero crater constructed by the Mars 2020 Science Team. *Space Science Reviews*, 216(8), 127. <https://doi.org/10.1007/s11214-020-00739-x>
- Sztanó, O., Magyar, Á., & Tóth, T. (2010). Gilbert-típusú delta a pannóniai Kállaai Kavics Tapolca környéki előfordulásaiban. *Földtani Kozlony*, 104(2), 167–182.
- Tate, C. D., Hayes, A. G., Kanine, O., Caravaca, G., Gupta, S., & Paar, G. (2024). Stratigraphic reconstruction and analysis of the delta remnant Kodiak in Jezero Crater, Mars. *ESS Open Archive*. <https://doi.org/10.22541/essoar.170688831.10785219/v1>
- Tate, C. D., Hayes, A. H., Kanine, O. A., Gupta, S., Caravaca, G., & Paar, G. (2023). Stratigraphic reconstruction and analysis of the delta remnant Kodiak in Jezero crater, Mars. In *54th lunar and planetary science conference* (p. 2782). The Woodlands. Retrieved from <https://www.hou.usra.edu/meetings/lpsc2023/pdf/2782.pdf>
- Tavani, S., Granado, P., Corradetti, A., Girundo, M., Iannace, A., Arbués, P., et al. (2014). Building a virtual outcrop, extracting geological information from it, and sharing the results in Google Earth via OpenPlot and Photoscan: An example from the Khaviz Anticline (Iran). *Computers & Geosciences*, 63, 44–53. <https://doi.org/10.1016/j.cageo.2013.10.013>
- Triantafyllou, A., Watlet, A., Le Mouélic, S., Camelbeeck, T., Civet, F., Kaufmann, O., et al. (2019). 3-D digital outcrop model for analysis of brittle deformation and lithological mapping (Lorette cave, Belgium). *Journal of Structural Geology*, 120, 55–66. <https://doi.org/10.1016/j.jsg.2019.01.001>
- Uličný, D. (2001). Depositional systems and sequence stratigraphy of coarse-grained deltas in a shallow-marine, strike-slip setting: The Bohemian Cretaceous basin, Czech republic. *Sedimentology*, 48(3), 599–628. <https://doi.org/10.1046/j.1365-3091.2001.00381.x>
- Ullman, S. (1979). The interpretation of structure from motion. *Proceedings of the Royal Society of London - Series B: Biological Sciences*, 203(1153), 405–426. <https://doi.org/10.1098/rspb.1979.0006>
- Van Yperen, A. E., Poyatos-Moré, M., Holbrook, J. M., & Midtkandal, I. (2020). Internal mouth-bar variability and preservation of subordinate coastal processes in low-accommodation proximal deltaic settings (Cretaceous Dakota Group, New Mexico, USA). *The Depositional Record*, 6(2), 431–458. <https://doi.org/10.1002/dep2.100>
- Viparelli, E., Blom, A., & Parker, G. (2012). Modeling stratigraphy formed by prograding Gilbert deltas. In *River flow 2012: The sixth edition of the international conference on fluvial hydraulics* (pp. 827–836). Taylor & Francis. San Jose, Costa Rica.
- Wentworth, C. K. (1922). A scale of grade and class terms for clastic sediments. *The Journal of Geology*, 30(5), 377–392. <https://doi.org/10.1086/622910>
- Wiens, R. C., & Maurice, S. (2021). Mars 2020 SuperCam bundle [Dataset]. *PDS*. <https://doi.org/10.17189/1522646>
- Wiens, R. C., Maurice, S., Robinson, S. H., Nelson, A. E., Cais, P., Bernardi, P., et al. (2020). The SuperCam instrument suite on the NASA Mars 2020 rover: Body unit and combined system tests. *Space Science Reviews*, 217(1), 4. <https://doi.org/10.1007/s11214-020-00777-5>
- Wilson, S. A., Moore, J. M., Howard, A. D., & Wilhelms, D. E. (2010). Evidence for ancient lakes in the Hellas region. In *Lakes on Mars* (pp. 195–222). Elsevier. <https://doi.org/10.1016/B978-0-444-52854-4.00007-6>
- Wilson, S. A., Morgan, A. M., Howard, A. D., & Grant, J. A. (2021). The global distribution of craters with alluvial fans and deltas on Mars. *Geophysical Research Letters*, 48(4), e2020GL091653. <https://doi.org/10.1029/2020GL091653>
- Xu, Z., Wu, S., Wang, Q., Zhang, P., Deng, M., Feng, W., et al. (2023). Internal architectural patterns of bar fingers within digitate shallow-water delta: Insights from the shallow core, GPR and Delft3D simulation data of the Ganjiang delta, China. *Lithosphere*, 2022(Special 13), 9120724. <https://doi.org/10.2113/2022/9120724>
- Yin, A. (2021). Glacial origin of landform assemblages in wester Jezero crater, Mars (pp. P251–2254). Retrieved from <https://ui.adsabs.harvard.edu/abs/2021AGUFM.P2512254Y>
- Zhang, J.-J., Wu, S.-H., Fan, T.-E., Fan, H.-J., Jiang, L., Chen, C., et al. (2016). Research on the architecture of submarine-fan lobes in the Niger delta basin, offshore West Africa. *Journal of Palaeogeography*, 5(3), 185–204. <https://doi.org/10.1016/j.jop.2016.05.005>
- Zhang, M., Zhao, J., Xiao, L., Xu, Y., Bugiolacchi, R., & Wang, J. (2023). Fan-shaped deposits in the northern Hellas region, Mars: Implications for the evolution of water reservoir and climate. *Icarus*, 395, 115470. <https://doi.org/10.1016/j.icarus.2023.115470>